

Caterina Lonati, Georgy Berezhnoy, Nathan Lawler, Reika Masuda, Aditi Kulkarni, Samuele Sala, Philipp Nitschke, Laimdota Zizmare, Daniele Bucci, Claire Cannet, Hartmut Schäfer, Yogesh Singh, Nicola Gray, Samantha Lodge, Jeremy Nicholson, Uta Merle\*, Julien Wist\* and Christoph Trautwein\*

# Urinary phenotyping of SARS-CoV-2 infection connects clinical diagnostics with metabolomics and uncovers impaired NAD<sup>+</sup> pathway and SIRT1 activation

https://doi.org/10.1515/cclm-2023-1017 Received September 12, 2023; accepted October 22, 2023; published online November 14, 2023

#### **Abstract**

**Objectives:** The stratification of individuals suffering from acute and post-acute SARS-CoV-2 infection remains a critical challenge. Notably, biomarkers able to specifically monitor viral progression, providing details about patient clinical status, are still not available. Herein, quantitative metabolomics is progressively recognized as a useful tool to describe the consequences of virus-host interactions considering also clinical metadata.

Julien Wist and Christoph Trautwein contributed equally to this work.

\*Corresponding authors: Uta Merle, Department of Internal Medicine IV, University Hospital Heidelberg, 69120 Heidelberg, Germany,

E-mail: Uta.Merle@med.uni-heidelberg.de; **Julien Wist**, Australian National Phenome Centre and Computational and Systems Medicine, Health Futures Institute, Murdoch University, 6150 Perth, Australia,

E-mail: Julien.Wist@murdoch.edu.au; and **Christoph Trautwein**, Werner Siemens Imaging Center, Department of Preclinical Imaging and Radiopharmacy, University Hospital Tübingen, 72074 Tübingen, Germany, E-mail: christoph.trautwein@med.uni-tuebingen.de. https://orcid.org/0000-0003-4672-6395 (C. Trautwein)

**Caterina Lonati**, Center for Preclinical Research, Fondazione IRCCS Ca' Granda Ospedale Maggiore Policlinico, Milan, Italy; and Werner Siemens Imaging Center, Department of Preclinical Imaging and Radiopharmacy, University Hospital Tübingen, Tübingen, Germany

**Georgy Berezhnoy, Aditi Kulkarni, Laimdota Zizmare and Daniele Bucci,** Werner Siemens Imaging Center, Department of Preclinical Imaging and Radiopharmacy, University Hospital Tübingen, Tübingen, Germany

Nathan Lawler, Reika Masuda, Samuele Sala, Philipp Nitschke, Nicola Gray, Samantha Lodge and Jeremy Nicholson, Australian National Phenome Centre and Computational and Systems Medicine, Health Futures Institute, Murdoch University Perth, Australia

**Claire Cannet and Hartmut Schäfer**, Bruker BioSpin GmbH, AIC Division, Ettlingen, Germany

**Yogesh Singh**, Institute of Medical Genetics and Applied Genomics, University Hospital Tübingen, Tübingen, Germany **Methods:** The present study characterized the urinary metabolic profile of 243 infected individuals by quantitative nuclear magnetic resonance (NMR) spectroscopy and liquid chromatography mass spectrometry (LC–MS). Results were compared with a historical cohort of noninfected subjects. Moreover, we assessed the concentration of recently identified antiviral nucleosides and their association with other metabolites and clinical data.

**Results:** Urinary metabolomics can stratify patients into classes of disease severity, with a discrimination ability comparable to that of clinical biomarkers. Kynurenines showed the highest fold change in clinically-deteriorated patients and higher-risk subjects. Unique metabolite clusters were also generated based on age, sex, and body mass index (BMI). Changes in the concentration of antiviral nucleosides were associated with either other metabolites or clinical variables. Increased kynurenines and reduced trigonelline excretion indicated a disrupted nicotinamide adenine nucleotide (NAD<sup>+</sup>) and sirtuin 1 (SIRT1) pathway.

**Conclusions:** Our results confirm the potential of urinary metabolomics for noninvasive diagnostic/prognostic screening and show that the antiviral nucleosides could represent novel biomarkers linking viral load, immune response, and metabolism. Moreover, we established for the first time a casual link between kynurenine accumulation and deranged NAD<sup>+</sup>/SIRT1, offering a novel mechanism through which SARS-CoV-2 manipulates host physiology.

**Keywords:** COVID-19; antiviral nucleosides; kynurenine pathway; sirtuins; precision diagnostics

#### Introduction

Despite the proven efficacy of vaccinations in preventing COVID-19 development, thereby reducing the rate of fatal events and hospitalizations, the SARS-CoV-2 outbreak still poses health, social, and economic challenges worldwide. In fact, the number of confirmed cases is globally increasing [1],

while a Nature survey conducted amongst immunologists, virologists, and infectious-disease experts indicated that SARS-CoV-2 will continue to circulate in the human population for years to come [2]. In addition, about 10-15% of patients who suffered from mild-to-moderate COVID-19 present persistent symptoms weeks or even months after the original infection [3]. This emerging clinical condition, referred to as post-acute COVID-19 syndrome (PACS), has the potential to overwhelm health systems and economies.

Although COVID-19 preferentially affects the respiratory tract, it is now well-established that systemic manifestations are a major component of the clinical picture. While viral spreading to extrapulmonary organs is mechanistically explained by the ubiquitous expression of the angiotensinconverting enzyme 2 (ACE2), disease outcome largely depends on host factors, including age, sex, and pre-existing comorbidities, as well as on the effectiveness of individual immune responses mounted to combat the infection [4, 5]. The wide spectrum of the possible virus-host interactions result in a substantial degree of heterogeneity in symptoms, severity, recovery time, and response to treatments [5-9].

Besides the broad dysregulation of inflammatory markers, it is now clear that multiple biochemical pathways are profoundly affected in COVID-19 [9-16]. Among the metabolic perturbations associated with SARS-CoV-2 infection, alterations in the kynurenine pathway represent the strongest metabolic signal observed so far [17-24]. Other widely-described abnormalities include metabolites related to tricarboxylic acid (TCA) and urea cycle, as well as glucose, phenylalanine, and the niacin metabolite trigonelline [17, 18, 22, 25]. Not only does metabolite dysregulation affect the initiation and maintenance of immune response [5, 13, 16, 26-28], but it can also be directly linked to specific COVID-19 pathological hallmarks, especially in the case of neurological symptoms and cardiovascular manifestations [18, 29, 30]. Given the crucial role of the metabolic phenotype in COVID-19, Holmes and coworkers introduced the concept of phenoreversion to describe the metabolic evolution associated with the disease [6] and demonstrated that incomplete recovery of metabolic homeostasis is associated to more severe symptoms [31]. With regard to the interplay between SARS-CoV-2 and the immune system, we recently identified novel urinary biomarkers, namely deoxy-didehydronucleosides (ddhNs), which are able to describe the activation of the host antiviral pathways in COVID-19 patients [32].

These observations collectively highlight the need to investigate the metabolic phenotype of COVID-19 patients further, as recognition of the specific metabotypes related to disease progression could have not only a descriptive value but also relevant diagnostic and prognostic significance. The

present study used a combination of proton nuclear magnetic resonance (<sup>1</sup>H NMR) spectroscopy and liquid chromatography-mass spectrometry (LC-MS) to investigate the urinary metabolic profiles associated with acute COVID-19 in a large cohort of patients that was previously characterized by serum metabolomics [11]. Urine was selected as biological matrix based on its valuable properties as non-invasively available biospecimen, which have been already recognized in the context of COVID-19 [19, 33-37]. The main focus of the present research was characterization of the acute COVID-19 urinary metabolic signature and recognition of the metabotypes specific to patient age, sex, and clinical deterioration. Further, we evaluated 4 ddhNs and their potential associations with either the other urinary metabolites or clinical parameters. In the final section of the study, we sought to expand knowledge on the SARS-CoV-2-induced changes in tryptophan metabolites and their involvement in the pathogenesis of the disease. More specifically, based on the crucial role of kynurenines in nicotinamide adenine dinucleotide (NAD) biosynthesis [38, 39], we explored whether a dysregulation in this pathway could affect the activation of the NAD+-dependent deacetylases known as sirtuins, which show potent immunomodulatory and antiviral properties [40-45].

#### Materials and methods

#### Study design

The present research investigated the metabolite profile of urine samples collected from Acute COVID-19 patients (AcuteCOV) (Heidelberg University Hospital). An independent pre-pandemic cohort of SARS-CoV-2-negative subjects was used as control (CTR) (data provided by Bruker BioSpin GmbH).

The overall study can be subdivided into 4 major aims: (1) Aim 1: Identification of the metabolite changes in AcuteCOV urine samples compared with CTR using <sup>1</sup>H NMR. This section analyzed the metabolite data obtained with <sup>1</sup>H NMR spectroscopy and Bruker IVDr method in urine samples to investigate differences between AcuteCOV (Werner Siemens Imaging Center, University Hospital Tübingen) patients and healthy CTR subjects (Data provided by Bruker BioSpin GmbH); (2) Aim 2: Characterization of the AcuteCOV urinary metabolic signature using <sup>1</sup>H NMR and LC–MS data. To enhance the characterization of AcuteCOV urinary metabolic phenotype, additional LC-MS experiments were carried out (Australian National Phenome Centre and Computational and Systems Medicine, Murdoch University). The information provided by this analysis integrated with the <sup>1</sup>H NMR data to derive more detailed metabolite profiles of AcuteCOV samples, which were then analyzed to identify potential disease severity, age, sex, BMI-dependent metabolic signatures; (3) Aim 3: Analysis of antiviral ddhNs and their associations with metabolite profiles and clinical variables. Here, we investigated whether the concentration of 4 antiviral ddhNs, namely 3'-deoxy3',4'-didehydro-cytidine (ddhC), 3'-deoxy-3',4'-didehydrocytidine-5'-carboxylic acid (ddhC-5'CA), 3'-deoxy-3',4'-didehydrouridine (ddhU), and 3',5'-dideoxy-3',4'-didehydrocytidine-5'-homocysteine (ddhC-5' Hcy), measured in urine samples by LC-MS, was associated with either variations in urinary metabolite concentration or changes in clinical parameters; (4) Aim 4: Investigation of the potential association between SARS-CoV-2-induced kynurenine pathway dysregulation, NAD+ biosynthesis, and sirtuins. In this section, we sought to provide a biological interpretation underlying the SARS-CoV-2-induced perturbations in the tryptophan metabolites, by investigating whether a dysregulation in this pathway could affect the activation of the NAD+dependent deacetylases sirtuins. To this aim, in addition to the results obtained by <sup>1</sup>H NMR and LC-MS in urine samples, we included the concentration of inflammatory mediators measured in matched serum samples of the same cohort of patients [11].

#### Study cohort information

Acute SARS-CoV-2 infected cohort (AcuteCOV): SARS-CoV-2 positive individuals were recruited from 7th September 2020 to 21st March 2021 within a prospective non-interventional study conducted by Heidelberg University Hospital [46]. According to the World Health Organization (WHO) guidance, laboratory confirmation for SARS-CoV-2 was defined as a positive result of quantitative real-time reverse transcriptase-polymerase chain reaction (qRT-PCR) assay of nasal and pharyngeal swabs. Only subjects who were over 18 years of age and showing completed questionnaires were included. All participants provided written informed consent according to the Declaration of Helsinki and the local Ethics committee had approved biosample and data collection and analysis (reference number: S-324/2020).

Patient management was based on ambulatory monitoring with the "Coronataxi digital early warning" (CDEW) system, deployed in Rhein-Neckar County and Heidelberg, Germany. This approach is an outpatient care system consisting of remote digital monitoring via a mobile application (with symptom questionnaire and daily pulse oximetry), a medical doctor dashboard and medical care delivery to COVID-19 patients in home quarantine when indicated (Heidelberg Medical University Ethics commission approval: S-324/2020).

Blood and urine sample collection took place during home visits by nurses. Upon collection, both blood and urine specimens were kept at room temperature (RT) and transferred to the Heidelberg University Hospital. Samples were then further processed and stored at -80 °C until shipment to the University of Tübingen Hospital.

Clinical data were collected based on structured patient interviews. The recorded information included the following variables: age, sex, medical comorbidities, regular medication, height, weight, severity of acute COVID-19 disease, symptoms. For hospitalized patients, the mode of respiratory support (oxygen supply via nasal low- or high-flow, oxygen mask or invasive mechanical ventilation) was likewise recorded.

Control (CTR) cohort: Urine metabolite patterns in healthy subjects have been characterized by Bruker BioSpin GmbH using a well-established quantitative in vitro diagnostics research (IVDr) standardized approach in <sup>1</sup>H NMR spectroscopy [47]. Healthy control urine samples were utilized for overall comparison and statistical investigations. In accordance with local requirements, informed permission was acquired from participants or their legal representatives.

#### Sample processing and quantitative <sup>1</sup>H NMR spectroscopy analysis

<sup>1</sup>H NMR spectra were generated using the standardized Bruker Avance IVDr platform (Avance III HD spectrometer) and the quantification was performed using the different Bruker IVDr packages (https://www.bruker.com/ de/products-and-solutions/mr/nmr-clinical-research-solutions/b-imethods.html), as previously described [48]. Urine sample preparation was performed according to B.I.-embedded standard operation procedure (SOP) [49]. For quality control (QC), the B.I. BioBank QC™ method; and for quantification B.I. Quant-UR eTM (e - extended, up to 150 metabolites quantified) modules were utilized. Briefly, for each sample a 600 µL aliquot was transferred into an autoclaved 2 mL microcentrifuge tube (MCT) and centrifuged at 2000 RCF for 10 min at 4°C (Heraeus Megafuge 8R, Thermo Electron LED GmbH, Osterode am Harz, Germany). Then, 585 μL of the supernatant were added with 65 μL of the standard Bruker urine buffer of pH 7.4 (order number AH0621-10. provided by Bruker BioSpin GmbH, Ettlingen, Germany; contains 1.5 M KH<sub>2</sub>PO<sub>4</sub>, 2 mM NaN<sub>3</sub>, 0.1 % TSP-d<sub>4</sub>) and the mixture was vortexed for 30 s (VORTEX-GENIE 2, Scientific Industries, Inc., Bohemia, NY, USA). A volume of 600 µL of the processed sample was then transferred to a 5 mm Bruker NMR tube.

NMR spectroscopy was performed using a 5 mm triple resonance (TXI) RT probe that was controlled via TopSpin software, version 3.6.2. The sample jet was set to a cooling temperature of 5 °C, then sample spectral data were acquired at 300 K. The standard one-dimensional (1D) NMR experiment with solvent suppression was acquired with 32 scans (65,536 data points, 20.0186 ppm spectral width). total experimental time of 4 min per sample. The obtained spectra were uploaded to the Bruker data analysis server for automated quantification. The sample and shim quality of the experiment was tested by the full width at half maximum (fwhm) of the TSP signal ( $\delta$  0.00) being less than 1.30 Hz, sharp singlet symmetrical peak. The residual water signal after solvent suppression is less than 30.0 mmol/L.

A statistical total correlation spectroscopy (STOCSY) was performed on each metabolite to find the signal patterns and their chemical shift [50]. Metabolites that could not be determined by its pattern and chemical shift by STOCSY were further investigated by 2D experiments (<sup>1</sup>H-<sup>1</sup>H COSY, <sup>1</sup>H-<sup>1</sup>H TOCSY, <sup>1</sup>H-<sup>13</sup>C HSQC and <sup>1</sup>H-<sup>13</sup>C HMBC). Each spectral region corresponding to the metabolites was integrated and correlated to the IVDr measurements to validate the quantification. Those that did not meet the criteria but the correct concentration is salvageable were done manually in R, otherwise removed from the analysis. Only metabolites passing the correlation of lineshape metabolite signals with calculated fit over 80 % were included in the study. Additionally, maleate quantification was excluded due to the recent report of urine NMR spectra in the same spectral region [32].

NMR metabolites were quantified via an external reference based on an ERETIC calibration [51]. The calibration transfer to each individual sample is facilitated by the PULCON principle [52]. An artificial reference peak representing a concentration equivalent of 10 mM can be added to the solvent suppressed 1D NMR spectrum in a region without metabolite signals. Quantitative calibrations need to be obtained and verified using a dedicated reference sample with known compound concentrations according to B.I. Methods QC procedures. Human body fluid sample preparation and NMR protocols were derived from an article of Dona et al. [49].

#### Sample processing and targeted quantitative LC-MS

Urine samples were thawed at 4 °C and prepared for analyses following previously reported metabolic phenotyping methods [53], with minor modifications. For the quantification of biogenic amines and amino acid metabolites, separation was performed by ultra-high-performance liquid chromatography (UHPLC) using an Acquity UPLC (Waters Corp, Milford, MA) coupled to a Bruker Impact II QToF mass spectrometer (Bruker, Daltonics, Billerica, MA). Resulting data files were processed for integrations and quantification using Target Analysis for Screening Quantification (TASQ) software v2.2 (Bruker, Daltonics, Bremen, Germany) where calibration curves were linearly fitted with a weighting factor 1/x. For the measurement of tryptophan and associated catabolites, separation was performed using Acquity UHPLC coupled to a Waters Xevo TO-XS mass spectrometer (Waters Corp. Wilmslow, U.K.). Obtained raw files were processed for peak integrations and metabolite quantifications using the TargetLynx package within MassLynx v4.2, where calibration curves were linearly fitted for each metabolites using a weighting factor of 1/x. Resulting data matrices were quality controlled and combined prior to statistical analysis.

#### Enzyme-linked immunoassay (ELISA) based analysis to assess serum SIRT1

SIRT1 serum concentration was measured with a commercially available Human SIRT1 ELISA Kit (Thermo Fisher Scientific Inc., Germany. Inter assay coefficient of variation <10 %, Intra assay coefficient of variation <12 %, detection limit: 1.23 ng/mL), according to the manufacturer's instructions. Serum samples of 171 patients were used in this experiment. Briefly, each well was filled with 50 µL of undiluted serum and  $50\,\mu L$  of proprietary diluent. Seven different concentrations of a lyophilized human SIRT1 standard were prepared to build a calibration curve ranging from 300 ng/mL to 1.229 ng/mL. Absorbance was measured at 450 nm using a plate Reader (Tecan Trading AG, Switzerland). SIRT1 concentration was then calculated based on the standard curve and by adjusting for sample dilution.

#### Statistical analysis and data interpretation

Statistical analysis was performed using the online comprehensive tool Metaboanalyst (Version 5.0), the JMP Pro 15 software (@SAS Institute Inc., Cary, NC, USA), and SigmaPlot 11.0 (Systat Software Inc., San Jose, CA, USA).

Missing values were handled by the replacement by limit of detection (LoDs) method (1/5th of the positive value of each variable). All spectra were baseline corrected and normalized using probabilistic quotient normalization (PQN) [54]. Both univariate and multivariate analysis approaches were applied. Unsupervised agglomerative hierarchical cluster analysis was performed to identify any potential specific signature of metabolite urine concentration (NA-chip analyzer program, https://sites.google.com/site/dchipsoft/). Unsupervised principal component analysis (PCA), supervised partial least squares discriminant analysis (PLS-DA) and orthogonal partial least squares - discriminant analysis (OPLS-DA) were also carried out as multivariate analysis. Differences across experimental groups were investigated by Mann-Whitney U test, Pearson's chi-squared test, One-way analysis of variance (ANOVA) or Kruskal-Wallis test on ranks. Two-way ANOVA was applied to investigate influences of two independent variables and their potential interaction. Tukey's test was used for post hoc multicomparison procedure. The false discovery rate (FDR) was controlled using the Benjamini-Hochberg correction to maximize statistical power [55]. Linear correlation between variables was assessed based on Pearson's correlation coefficient. A p-value <0.05 and a fold change (FC) >1.2 were considered significant.

The graphical abstract was generated via the biorender.com service with the help of standard COVID-19 related template (World Health Organization. https://www.who.int/emergencies/diseases/ novel-coronavirus-2019).

#### Results

#### Baseline characteristics of the study cohorts and metabolic data included in the analysis

A schematic workflow diagram of the investigation is shown in Figure 1.

#### Study sample

A subset of 243 individuals from the Coronataxi study, for whom there complete metadata as well as urine and blood samples collected at the first follow-up timepoint, was used for the purpose of this study. Concerning the CTR group, 309 subjects were extracted from the Bruker cohort and included in the present research. Demographic data of the two study groups are reported in Table 1. Age ranges were defined according to the following criteria [56]: young adult, from 19 to 24 years; adult, from 25 to 44 years; middle aged, from 45 to 64 years; aged, from 65 to 79 years; senile, >80 years. Body mass index (BMI) categories were likewise assigned based on standard classification: (1) underweight, BMI $\leq$ 18.5 kg/m<sup>2</sup>; (2) normal weight, BMI $\geq$ 18.5 and  $\leq$ 24.9 kg/m<sup>2</sup>; (3) overweight, BMI≥25 and ≤29.9 kg/m<sup>2</sup>; (3) obesity I, BMI>30 and  $\leq 34.9 \text{ kg/m}^2$ ; (4) obesity II, BMI>35 and  $\leq 39.9 \text{ kg/m}^2$ ; (5) obesity III, BMI>40 kg/m<sup>2</sup> [57]. Table 2 shows the baseline characteristics, clinical outcomes, laboratory data, and comorbidities of the AcuteCOV cohort.

#### Metabolic data

Up to 150 low-molecular-weight metabolite concentrations were obtained from the Bruker IVDr quantification in urine B.I.Quant-UR. The dataset was then subjected to internal QC analysis as described in the Methods: (1) Rho-sigma filtering; (2) metabolite detection in at least 70 % of the evaluated patient samples; (3) correlation of lineshape QC with calculated fit over 80 %. Based on these criteria, 44 metabolites were selected to be part of the final metabolite list for the

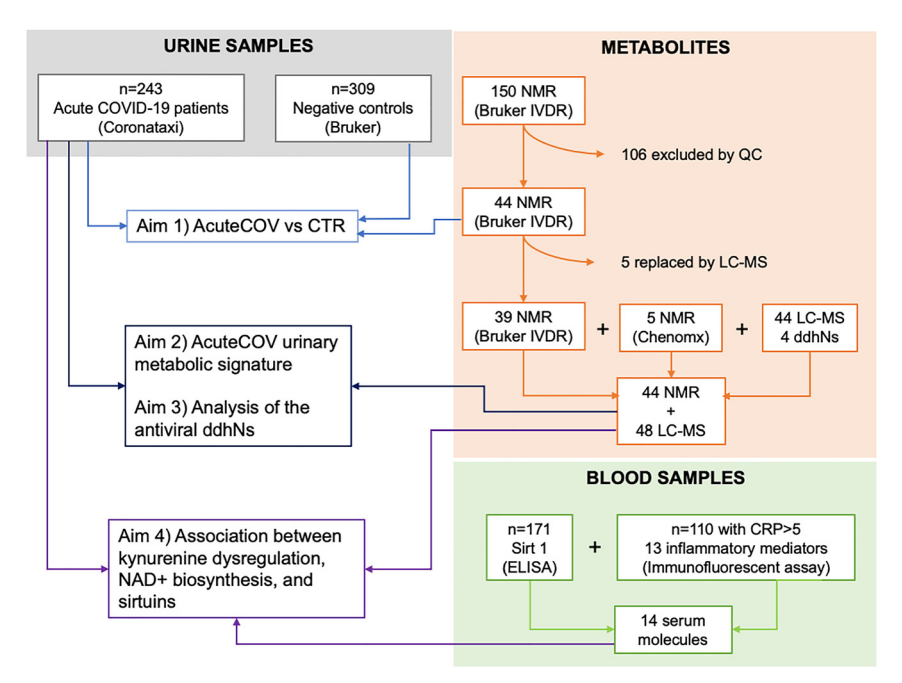


Figure 1: Consort diagram. Urine metabolomics was performed by <sup>1</sup>H NMR spectroscopy and LC-MS in a large cohort of SARS-CoV-2 infected individuals (n=243). The study is structured in 4 different consecutive aims. In addition to urinary metabolite profiles. Aim 4 involved the investigation of SIRT1 concentration in matched serum samples. Thirteen inflammatory mediators, whose concentration was measured within our previous study [11], were likewise included in the present analysis. AcuteCOV, Acute COVID-19 cohort; CRP, C-reactive protein; CTR, controls; ddhNs, deoxy-didehydronucleosides; LC-MS, liquid chromatography-mass spectrometry; NAD+, nicotinamide adenine dinucleotide; NMR, nuclear magnetic resonance; QC, quality control; SIRT1, sirtuin 1.

**Table 1:** Demographic information of the AcuteCOV and CTR study cohorts.

	Study cohorts			
	CTR (n=309)	AcuteCOV (n=243)	p-Value	
Gender group, n (%)			0.548	
F	151 (27.3 %)	125 (22.6 %)		
M	158 (28.6 %)	118 (21.3 %)		
Age, years	$53.5 \pm 14.4$	$52.8 \pm 14.3$	0.042	
Age group, n (%)			0.053	
Young adult	5 (0.9 %)	6 (1.0 %)		
Adult	76 (13.7 %)	66 (11.9 %)		
Middle aged	174 (31.5 %)	121 (21.9 %)		
Aged	34 (6.1 %)	43 (7.7 %)		
Senile	20 (3.6 %)	7 (1.2 %)		
BMI, kg/m²	$26.00 \pm 4.00$	28.61 ± 6.19	< 0.001	
BMI group, n (%)			0.013	
Underweight	3 (1 %)	3 (1.39 %)		
Normal weight	132 (44 %)	70 (32.55 %)		
Overweight	122 (40.66 %)	66 (30.69 %)		
Obesity class I	35 (11.66 %)	47 (21.86 %)		
Obesity class II	6 (2 %)	23 (10.69 %)		
Obesity class III	2 (0.66 %)	9 (4.18 %)		

Data are expressed as mean±standard deviation or n (%). p-Values were calculated by Wilcoxon test or Pearson's chi-squared test when appropriate. BMI, body mass index; AcuteCOV, acute COVID.

comparison of AcuteCOV vs. CTR (Aim 1, Figure 1; please find the complete list in Supplementary Table S1).

With regard to aims 2, 3, and 4 the concentrations of alanine, glycine, methionine, taurine, and valine provided by NMR spectroscopy experiments were replaced with the

corresponding LC–MS-based data (Figure 1, Supplementary Table S1, metabolites highlighted in green color). Moreover, 5 additional metabolites (3-indoxylsulfate, hypoxanthine, pseudouridine, urea, cis-aconitate) were manually analyzed using Chenomx NMRSuite 7.1. Therefore, the final list for aims 2, 3, and 4 included 92 metabolites, out of which 44 were measured by NMR and 48 by LC–MS (Figure 1; please find the complete list in Supplementary Table S1).

## Aim 1: Identification of the metabolite changes in AcuteCOV urine samples compared with CTR

PCA was carried out to investigate general group separation based on urinary metabolite concentrations assessed via <sup>1</sup>H NMR spectroscopy-based metabolomics approach (Figure 2A). Unsupervised hierarchical clustering revealed a good discrimination between the urinary metabolite profile of AcuteCOV and CTR groups (Supplementary Material 1.2.1). Associations between metabolite concentration profiles were explored by multivariate analysis that disclosed 13 main clusters of variables (Supplementary Material 1.2.1.2, Supplementary Table S2). Univariate analysis identified a total of 22 differentially expressed metabolites, of which 11 were increased in the AcuteCOV group compared with CTR, while 11 metabolites were decreased (Figure 2B).

Next, we investigated whether sex, age, and BMI factors can influence the metabolite changes associated with SARS-CoV-2 infection. Unsupervised hierarchical clustering

Table 2: Baseline characteristics of the AcuteCOV cohort.

	AcuteCOV cohort			
	Whole sample	Men		
	(n=243)	(n=125)	(n=118)	
Demographics				
Age, years	52.82 ± 14.3	$50.08 \pm 14.79$	55.72 ± 13.21	
BMI, kg/m <sup>2</sup>	$28.61 \pm 6.19$	$28.19 \pm 6.77$	29.07 ± 5.47	
Comorbidities				
Diabetes	28 (11.57 %)	8 (6.45 %)	20 (16.94 %)	
Asthma	34 (13.99 %)	26 (20.8 %)	8 (6.77 %)	
COPD	10 (4.11 %)	5 (4 %)	5 (4.23 %)	
Clinical outcomes				
Hospital admission	57 (23.45 %)	18 (14.4 %)	39 (33.05 %)	
Oxygen saturation <sup>b</sup>	$93.84 \pm 2.95$	94.15 ± 3.55	93.5 ± 2.07	
Oxygen demand	37 (64.91 %)	10 (55.55 %)	27 (69.23 %)	
ICU	6 (10.52 %)	2 (11.11 %)	4 (10.25 %)	
Body temperature <sup>a</sup> , °C	37.58 ± 1.04	$37.49 \pm 0.98$	37.67 ± 1.1	
Clinical laboratory				
CRP <sup>c</sup> , mg/dL	27.86 ± 39.11	21.97 ± 33.66	34.11 ± 43.44	
LDH <sup>c</sup> , U/L	280.93 ± 108.22	266.91 ± 107.86	295.79 ± 107.05	
AST <sup>c</sup> , U/L	36.1 ± 40.59	28.48 ± 19.88	43.72 ± 52.91	
Glucose <sup>a</sup> , mg/dL	100.16 ± 30.44	96.53 ± 29.62	103.99 ± 30.94	
Creatinine <sup>a</sup> , mg/dL	$0.8 \pm 0.23$	$0.67 \pm 0.14$	0.93 ± 0.24	
GFR <sup>a</sup> , mL/min	96.25 ± 19.36	101.51 ± 18.82	90.8 ± 18.47	
Hemoglobin <sup>a</sup> , g/dL	14.26 ± 1.47	13.67 ± 1.15	14.88 ± 1.52	
Transferrin <sup>a</sup> , g/L	$2.13 \pm 0.46$	$2.25 \pm 0.48$	2.01 ± 0.41	
Transferrin saturation <sup>a</sup> , %	18.27 ± 11.49	17.59 ± 11.92	18.99 ± 11.03	
Ferritin <sup>a</sup> , ng/mL	333.43 ± 446.84	152.39 ± 172.78	522.62 ± 555.28	
D-Dimer <sup>c</sup> , mg/L	1.06 ± 2.61	0.91 ± 1.33	1.23 ± 3.49	
Platelets <sup>a</sup> , ×10 <sup>3</sup> cells/µL	230.14 ± 147.15	253.59 ± 188.08	197.84 ± 75.26	
Leukocytes <sup>b</sup> , ×10 <sup>9</sup> cells/L	5.38 ± 2.18	5.33 ± 1.93	5.43 ± 2.41	
Lymphocytes <sup>b</sup> , ×10 <sup>9</sup> cells/L	$1.41 \pm 0.7$	$1.47 \pm 0.67$	1.35 ± 0.73	
Urea <sup>c</sup> , mg/dL	$30.58 \pm 30.84$	24.32 ± 8.34	32.92 ± 33.94	
Presence of urine proteins <sup>a</sup>	73 (30.41 %)	30 (24.19 %)	43 (37.06 %)	
Presence of urinary ketone bodies <sup>a</sup>	63 (26.25 %)	27 (21.77 %)	36 (31.03 %)	
Concurrent therapy	,	,	,	
Steroids	8 (3.29 %)	6 (4.8 %)	2 (1.69 %)	
L-Thyroxin	29 (11.93 %)	22 (17.6 %)	7 (5.93 %)	
DOACs	14 (5.76 %)	5 (4 %)	9 (7.62 %)	
Immunosuppression	4 (1.64 %)	1 (0.8 %)	3 (2.54 %)	
Hypertension	84 (34.56 %)	39 (31.2 %)	45 (38.13 %)	
Allopurinol	8 (3.29 %)	0 (0 %)	8 (6.77 %)	

Data are expressed as mean±standard deviation or n (%). AST, aspartate transaminase; BMI, body mass index; COPD, chronic obstructive pulmonary disease; CRP, C-reactive protein; DOAC, direct oral anticoagulants; GFR, glomerular filtration rate; ICU, intensive care unit; LDH, lactate dehydrogenase. <sup>a</sup>Measured on the day of urine collection; <sup>b</sup>minimum value; <sup>c</sup>maximum value (peak). Conversion factors to SI units: CRP, 1 mg/dL corresponds to 10 mg/L; glucose: 1 mg/mL corresponds to 0.056 mmol/L; creatinine, 1 mg/dL corresponds to 88.402 µmol/L; hemoglobin, 1 g/dL corresponds to 10 g/L.

analysis of metabolite concentrations disclosed a diseasedriven clusterization, indicating that the distinctive infection-dependent metabolic signature previously identified was sustained irrespective of age (Figure 2C, Supplementary Figure S1), sex (Figure 2D, Supplementary Figure S2), and BMI (Figure 2E). Consistently, for most of the differentially-expressed metabolites, the magnitude and pattern of modulation was similar to those observed within the whole sample analysis (Supplementary Table S3 and S4). However, some metabolites showed a different degree of modulation across demographic factors (sex, age, and BMI). Among these, taurine (p-value of interaction=0.042) and creatine (p=0.041) were differentially modulated between sex groups (Supplementary Table S3), whilst orotic acid (p=0.048), citric acid, (p=0.001), trigonelline (p=0.048), and glycine (p=0.009) showed different concentrations across age groups (Supplementary Table S3). Of note, lactic acid and succinic acid appeared to be modulated by both sex and age

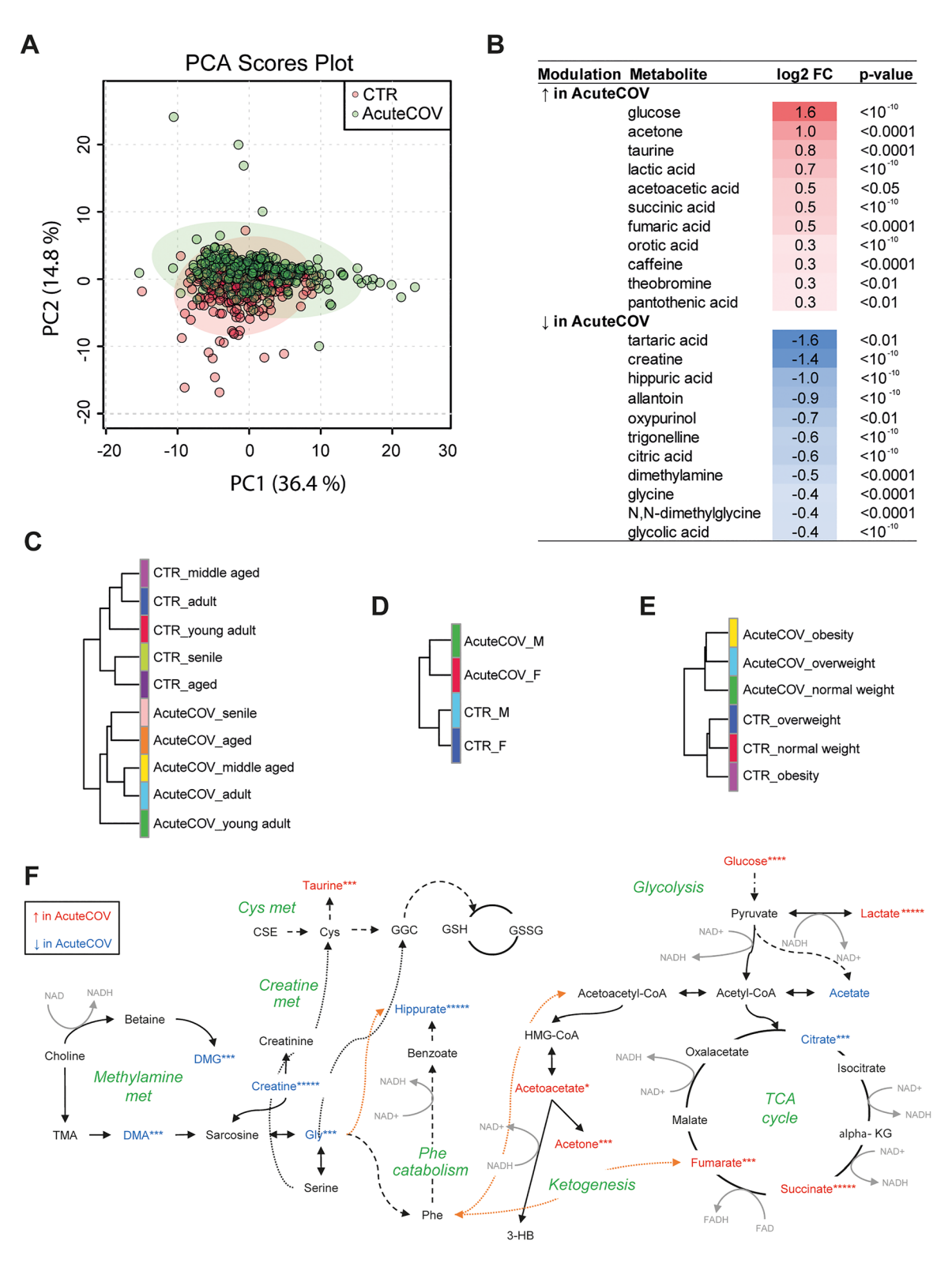


Figure 2: Identification of the metabolite changes in AcuteCOV urine samples compared with CTR. (A) Principal component analysis (PCA) scores plot illustrating general group separation based on urinary metabolite concentrations assessed via <sup>1</sup>H NMR spectroscopy-based metabolomics approach. The analysis excluded 4 patients based on extremely different glucose and creatinine urinary concentrations. Out of the 4 outliers, 3 were controls, while 1 subject was from the AcuteCOV group. (B) List of metabolites increased or decreased in AcuteCOV compared with CTR. Only molecules showing log2 fold change (FC) >1.2 are included. A two-color scale is used to illustrate FC: deep red denotes +1.6, deep blue denotes –1. Wilcoxon–Mann–Whitney test. Unsupervised hierarchical clustering reveals an overall SARS-CoV-2 infection-driven clusterization irrespective of (C) age, (D) sex, and (E) BMI groups.

factors. Moreover, two additional classes of modulation were identified: (1) different response to SARS-CoV-2 infection across sex groups, including syringic acid (p-value of interaction <0.001), erythritol (p=0.048), and pantothenic acid (p=0.033); (2) different response to SARS-CoV-2 infection across age groups, including formic acid (p=0.001) and inosine (p=0.045). Concerning BMI, the changes induced by SARS-CoV-2 were similar across BMI groups for most of the evaluated metabolites, except for succinic acid (p-value of interaction=0.036), oxypurinol (p=0.009), dimethylamine (p=0.031), glycolic acid (p=0.019), pantothenic acid (p=0.026), and inosine (p=0.043) (Supplementary Table S4).

The metabolites differentially modulated between AcuteCOV and CTR groups were manually assigned to the following major metabolic pathways: (1) drug/food metabolite (n=5): caffeine, theobromine, pantothenic acid, oxypurinol, tartaric acid; (2) TCA cycle (n=4): succinic acid, fumaric acid, citric acid, glycolic acid; (3) one-carbon metabolism (n=3): dimethylamine, N,N-dimethylglycine, glycine; (4) fasting/ketogenesis (n=2): acetone, acetoacetic acid; (5) glucose homeostasis (n=2): glucose, lactic acid; (6) cysteine oxidation/creatine metabolism (n=2): taurine, creatine; (7) pyrimidine de novo synthesis/urea cycle (n=2): orotic acid, allantoin; (8) phenylalanine catabolism (n=1): hippuric acid; (9) nicotinic acid metabolism (n=1): trigonelline. Of interest, "one-carbon metabolism" includes only down-regulated metabolites, while "fasting/ketogenesis" and "glucose homeostasis" involve only increased molecules. Figure 2F illustrates the metabolic pathways enriched of modulated metabolites. Enrichment pathway analysis demonstrated a significant similarity to the diabetes mellitus metabolic signature (8 hits over 19 total metabolites, FDR-adjusted p-value:  $7.78 \times 10^{-8}$ ).

#### Aim 2: Characterization of the AcuteCOV urinary metabolic signature

To further investigate the metabolic changes elicited during SARS-CoV-2 infection, the AcuteCOV urine samples were analyzed using LC-MS at the Australian National Phenome Centre, Murdoch University. As reported in Supplementary Table S1, we measured 44 additional metabolites and 4 antiviral ddhNs: ddhC, ddhC-5'CA, ddhC-5'Hcy, and ddhU [32].

#### Association between urine metabolic profiles and disease severity

#### Differences in the urinary metabolite concentration between hospitalized and nonhospitalized patients

We explored metabolite differences between non-hospitalized (n=186) and hospitalized (n=57) patients. Univariate analysis identified 12 up-regulated metabolites in the hospitalized group, among which there were the antiviral nucleosides and 4 metabolites involved in the tryptophan catabolic pathway, namely 3-hydroxykynurenine, kynurenine, 3-hydroxyanthranilic acid, and quinolinic acid (Supplementary Table S5). On the other hand, 8 metabolites, including citric acid, trigonelline, allantoin, and glycine were down-regulated in hospitalized patients compared with subjects who did not require hospital admission.

To depict the clinical significance of the identified metabolite differences, a volcano plot was created using both metabolites and clinical data. As shown in Figure 3, C-reactive protein (CRP) and ferritin serum concentrations showed similar fold change range and degree of statistical significance compared with the antiviral ddhNs, 3-hydroxykynurenine, and kynurenine. With regard to variables with reduced concentrations in the hospitalized compared with the nonhospitalized group, iron, citric acid, lymphocyte count, Transferrin saturation, glomerular filtration rate (GFR), platelets, and glycine, showed the most significant p-values.

Finally, we carried out a biomarker analysis based on area under ROC curve (AUC) calculation (Supplementary Figure S3). Peak CRP showed the greater discrimination ability between hospitalized and nonhospitalized patients (AUC: 0.802(0.743–0.862), specificity: 0.785(0.731–0.842)), sensitivity: 0.737(0.622-0.834)), followed by 3-hydroxy kynurenine (AUC: 0.766(0.694–0.840, specificity: 0.763(0.707– 0.817), sensitivity: 0.719(0.614–0.816)), and kynurenine (AUC: 0.7654(0.691–0.829), specificity: 0.715(0.642–0.769), sensitivity: 0.737(0.613-0.851)). Of note, the best performance in this population was provided by the ratio between platelets and peak CRP that showed an AUC of 0.837 (0.767-0.898) (Supplementary Figure S3).

#### Recognition of metabolic signatures associated with clinical deterioration

Metabolic profiles were analyzed according to the serum concentration of biomarkers currently used in the clinical

<sup>(</sup>F) Simplified diagram illustrating the dysregulated metabolites and their interactions. Increased metabolites in AcuteCOV vs. CTR are typed with red letters, while down-regulated with blue letters. Metabolites typed with black letters show similar concentration across study groups. Wilcoxon-Mann-Whitney test, p-values: \*\*\*\*\* <10<sup>-10</sup>; \*\*\*\* <10<sup>-8</sup>; \*\*\* <10<sup>-4</sup>; \*\* <0.01; \*<0.05. BMI, body mass index; Cys, cysteine; FC, fold change; met, metabolism; Phe, phenylalanine; TCA, tricarboxylic acid.

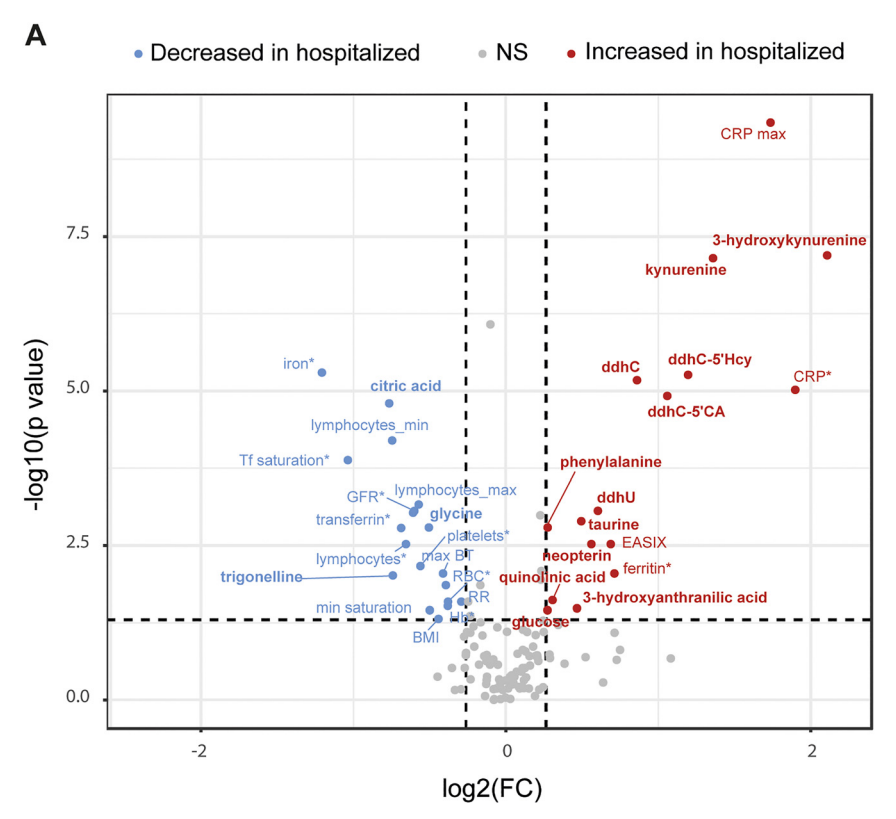


Figure 3: Differences in urinary metabolite concentration and serum clinical parameters between hospitalized and nonhospitalized patients. (A) Combined volcano plot showing the metabolites and the clinical variables significantly different in the comparison of hospitalized (n=57) vs. nonhospitalized (n=186) patients, with a fold change >1.2 and p-value <0.05. Increased variables are typed with red letters, while decreased with blue letters. Metabolites are written in bold, while clinical parameters are diplayed in a regular typeface. \*Denotes serum variables assessed on the same day of urine collection. BMI, body mass index; BT, body temperature; CRP, C-reactive protein; EASIX, endothelial activation and stress index; GFR, glomerular filtration rate; RR, respiratory rate; Tf, transferrin.

practice to evaluate the main pathophysiological derangements leading to severe disease. Notably, based on previous studies [58, 59], we elected to use the following clinical variables: CRP (inflammation), peripheral blood lymphocyte count (immune response), D-dimer (coagulation), and oxygen saturation (SpO2, lung function). We also included the Endothelial activation and stress index (EASIX), a predictor of endothelial complications recently validated in a cohort of COVID-19 hospitalized patients [60]. As shown in the heatmap reported in Figure 4, two main clusters were identified (euclidean distance measure, ward clustering): (1) metabolites whose concentration tend to increase along with worsening of clinical parameters; (2) metabolites whose concentration tend to decrease along with worsening of clinical parameters. As highlighted in the dendogram of the hierarchical cluster analysis, each of the two main clusters included two sub-clusters, referred to as 1A (n=2 metabolites), 1B (n=11), 2A (n=7), and 2B (n=9). Of note, Cluster 1B includes the tryptophan-related metabolites neopterin, 3-hydroxy kynurenine, kynurenine, and 3-hydroxyanthranilic acid, together with the 4 antiviral ddhNs.

#### Influences of sex, age, and BMI factors on the AcuteCOV metabolomic profile

We investigated whether specific metabolite profiles could be identified across sex, age, and BMI patient subgroups.

Compared with women, men had higher concentrations of xanthurenic acid, tryptophan, 3-hydroxykynurenine,

tyrosine, kynurenine (Supplementary Figure S4A). Conversely, female urine showed higher amounts of a number of organic acids, including lactic acid, citric acid, indole-3-acetic acid, beta-aminoisobutyric acid, succinic acid, glutamic acid, acetic acid, aspartate, and fumaric acid (Supplementary Figure S4A).

Investigation of the metabolite differences across age groups disclosed increasing concentrations of neopterin, ddhC-5'CA, and taurine as the population increases in age, since lower levels of these metabolites were observed in younger subjects compared with the senile group (Supplementary Figure S4B). Of note, the same pattern of modulation was observed for the metabolites related to the tryptophan pathway, including kynurenine, quinolinic acid, 3-hydroxykynurenine, and kynurenic acid (Supplementary Figure S4B).

Finally, healthy-weight range patients displayed increased urinary concentrations of glycine, citric acid, indole-3.-acetic acid, and serine compared with subjects with higher BMI, whereas inosine, tyrosine, 1-methylhistidine showed an opposite modulation pattern (Supplementary Figure S5).

### Aim 3: Analysis of the antiviral ddhNs and their associations with metabolite profiles and clinical variables

The 4 antiviral molecules ddhC, ddh-5'CA, ddhC-5'Hcy, ddhU accounted for a significant proportion of variability in the

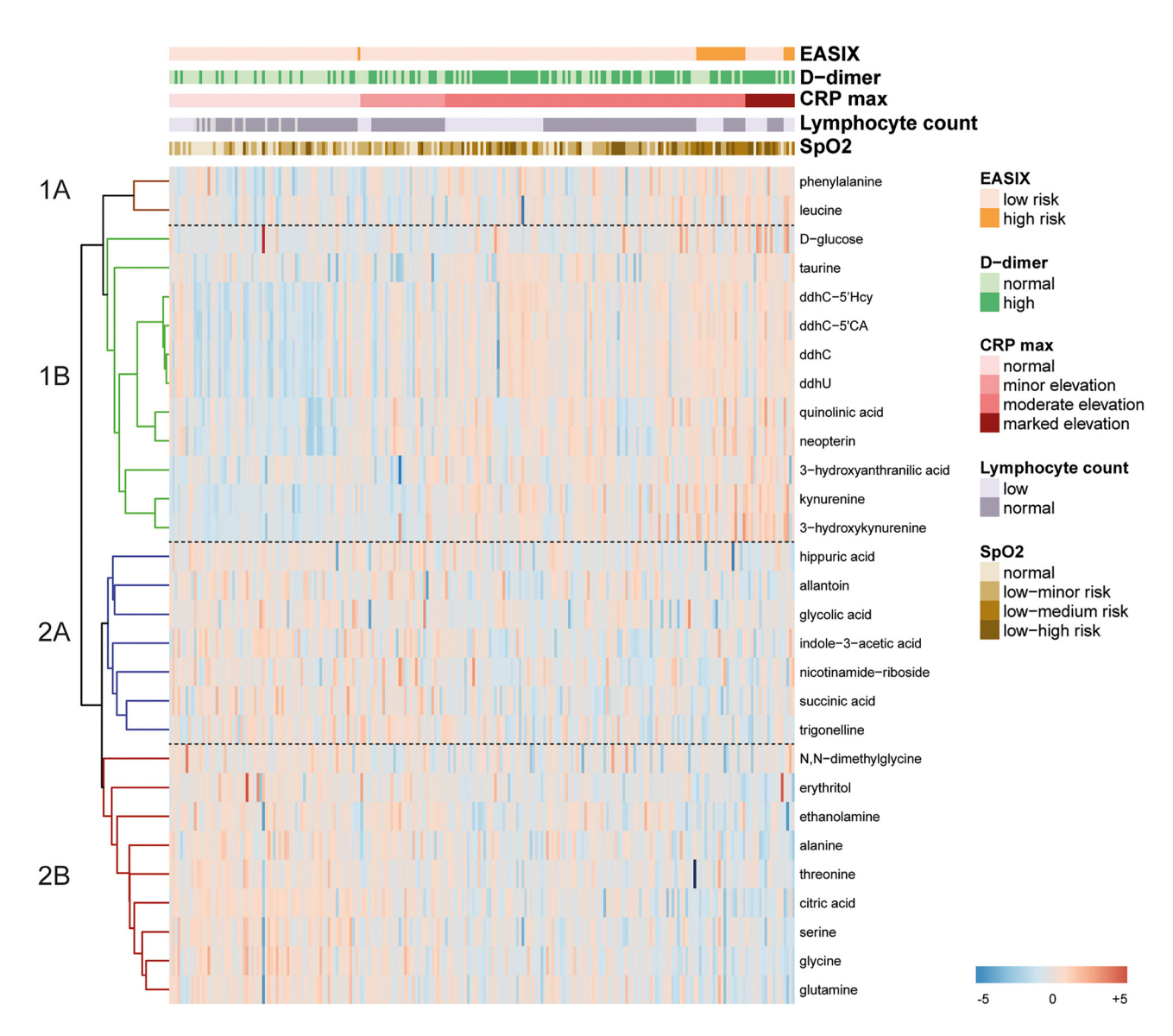


**Figure 4:** Recognition of urinary metabolic signatures associated with clinical deterioration. Heatmap showing the concentration of those metabolites which resulted significantly different across the following classes of clinical variables: EASIX; low risk, vs. high risk; D-dimer: normal vs. high; CRP: normal vs. minor elevation, vs. moderate elevation vs. marked elevation; lymphocyte count: normal vs. low; SpO<sub>2</sub>: normal vs. low-minor risk vs. low-medium risk vs. low-high risk. Clustering method: average linkage; distance metric: 1–Spearman's rank correlation. Four main metabolite signatures are identified: (1A) (orange dendrogram), (1B) (green), (2A) (violet), (2B) (brown). A two-color scale is used to illustrate the metabolite modulation pattern: deep red denotes +5, deep blue denotes –5. Specific color-coded scales denote the different clinical parameters and their classes. CRP, C-reactive protein; EASIX, endothelial activation and stress index; SpO<sub>2</sub>, oxygen saturation.

dataset, as indicated by PCA (Figure 5A). Thus, we explored whether these molecules were related to specific metabolite signatures and clinical manifestations. To this end, a combined factor, referred to as "Total ddhNs", was calculated for each patient by adding up the urinary concentration of the 4 anti-viral nucleosides: [ddhC] + [ddh-5'CA] + [ddh-5'Hcy] + [ddhU]. As shown in Table 3, "Total ddhNs" was positively associated with markers of systemic inflammation, including CRP, EASIX, and LDH, whereas leukocytes and lymphocyte counts decreased along with increasing antiviral nucleoside

concentrations. With regard to associations with the other metabolites, a strong positive correlation was found with neopterin and a number of molecules related to tryptophan metabolism, including quinolinic acid. kynurenine, 3-hydroxykynurenine, kynurenic acid, and 3-hydroxyanthranilic acid (Table 4). On the other hand, citric acid, glycine, and threonine showed the lowest correlation coefficients, indicating an inverse association with antiviral nucleosides. Moreover, an inverse correlation was observed between the nucleoside sum and different glucogenic amino

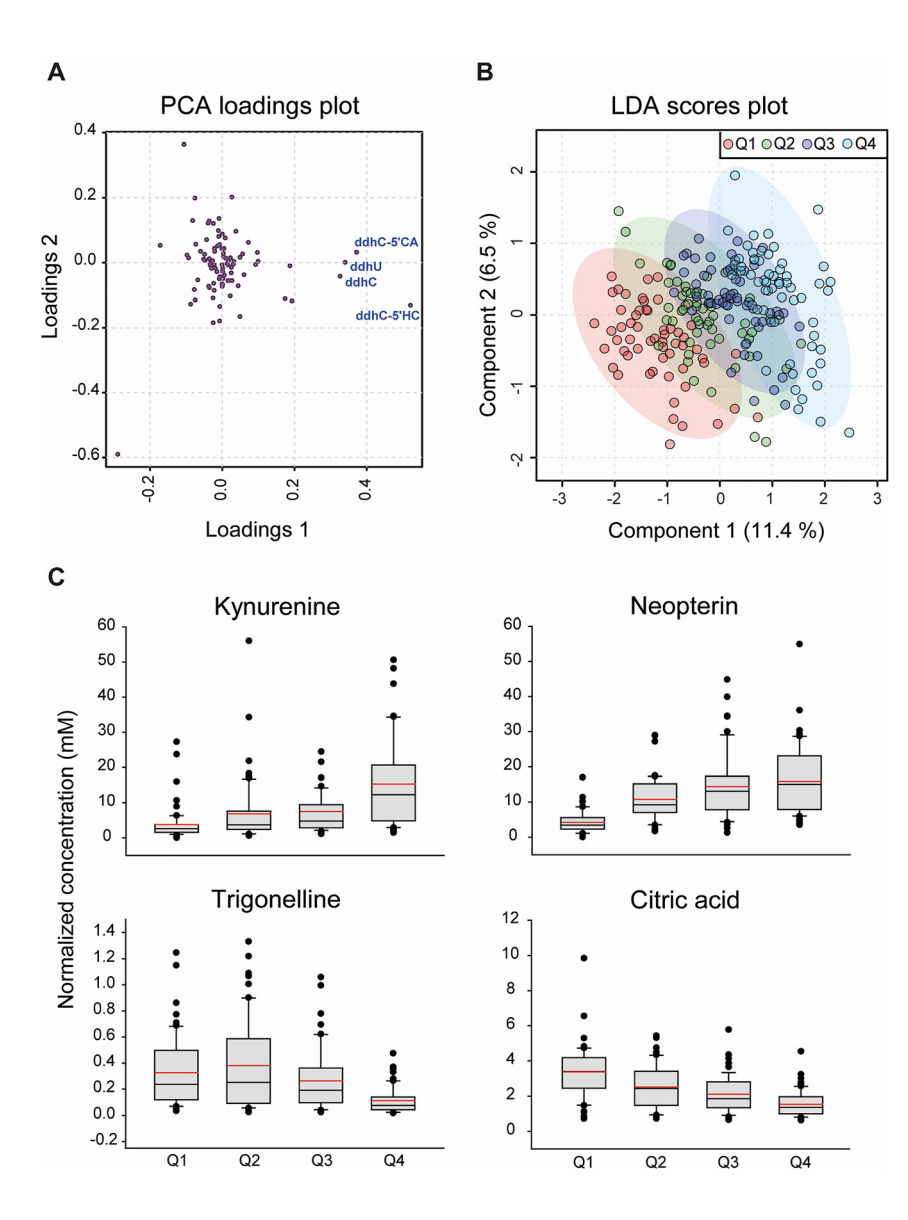


Figure 5: Analysis of the antiviral ddhNs and their associations with metabolic urinary profiles. (A) Principal component analysis (PCA) loading plot showing a strong influence of the 4 ddhNs on PC1. (B) PLS-DA reveals no overlap between the quartile Q1 and Q4 of "Total ddhNs", which was calculated for each patient by adding up the urinary concentrations of the 4 antiviral nucleosides: [ddhC] + [ddh-5' CA] + [ddhC-5'Hcy] + [ddhU]. (C) Box plots illustrating the metabolites with the highest fold change between "Total ddhNs" Q1 and Q4. Kruskal-Wallis One-way ANOVA on Ranks. Normalized concentrations were obtained by applying the probabilistic quotient normalization (PQN). All the metabolites displayed here had a p-value<0.001. For each experimental group, box plots show the median [25-75], while the red line denotes the mean. LDA, linear discriminant analysis; PCA, principal component analysis; Q, quartile.

acids entering the TCA cycle upstream to succinate, such as glycine, serine, threonine, alanine, arginine, glutamine, whereas aspartate, which is converted to oxaloacetate, resulted positively correlated.

To further understand the association between the antiviral nucleosides and the concentration of the other metabolites, we stratified the population according to quartiles (Q) of "Total ddhNs": (1) Q1, from 0.1 AU to 214.6 AU; (2) Q2, from 214.6 AU to 756.7 AU; (3) Q3, from 756.7 AU to 2,220.9 AU; (4) Q4, from 2,220.9 AU to 6,939.4 AU. PLS-DA found an excellent discrimination between Q1 and Q4 (Figure 5B). These results were confirmed by univariate analysis performed to investigate differences in the metabolite concentrations across the quartiles (Figure 5C and Supplementary Table S6). Among the metabolites whose concentration increased along with higher "Total ddhNs", kynurenine, neopterin, 3-hydroxykynurenine,

and quinolinic acid showed the highest FC between Q1 and Q4. Conversely, the reduced metabolites were citric acid and trigonelline.

## Aim 4: Investigation of the potential association between SARS-CoV-2-induced kynurenines/trigonelline dysregulation, NAD+ biosynthesis, and sirtuins

As schematized in Figure 6A, the kynurenine pathway mediates NAD<sup>+</sup> *de novo* synthesis from tryptophan. Since SARS-CoV-2 can inhibit NAD<sup>+</sup> generation through downregulation of the enzymes NAD Synthetase 1 (NADSYN1) and quinolate phosphoribosyltransferase (QPRT) [61], the

Table 3: Association between "Total ddhNs" and clinical variables.

Table 4: Association between "Total ddhNs" and the other urinary metabolites.

Group	Variable	Total ddhNs				Takal J.B.At.	
		r	p-Value	Pathway	Metabolites	Total ddhNs	
Demographic data						r	p-Value
	Age	0.13	<0.05	Immune response			
	BMI	0.06	ns		Neopterin	0.66	< 0.0000
	HOMA-IR	-0.02	ns	Tryptophan metabolism			
Systemic inflammatory					Quinolinic acid	0.51	< 0.0000
response					Kynurenine	0.48	<0.0000
	CRP <sup>c</sup>	0.37	< 0.00001		3-Hydroxykynurenine	0.43	<0.0000
	EASIX <sup>a</sup>	0.38	< 0.00001		Kynurenic acid	0.24	<0.000
	LDH <sup>c</sup>	0.29	<0.0001		3-Hydroxyanthranilic	0.22	< 0.000
	Ferritin <sup>a</sup>	0.14	<0.05		acid		
Immune function					Indole-3-acetic acid	-0.22	< 0.00
	Leukocytes <sup>a</sup>	-0.22	<0.001	Ketogenesis			
	Leukocytes <sup>b</sup>	-0.38	< 0.00001	_	Acetone	0.30	< 0.0000
	Lymphocytes <sup>a</sup>	-0.24	<0.001	Phenylalanine			
	Lymphocytes <sup>b</sup>	-0.31	<0.00001	metabolism			
	Neutrophiles <sup>a</sup>	-0.25	< 0.0001		Phenylalanine	0.24	<0.00
Blood coagulation and	·				Dopamine	0.22	<0.00
fibrinolysis				Cysteine oxidation/crea-			
•	D-Dimer <sup>c</sup>	0.12	ns	tine metabolism			
	Platelets <sup>a</sup>	-0.29	<0.00001		Taurine	0.42	< 0.0000
	INR <sup>a</sup>	-0.18	<0.01		Creatinine	0.28	< 0.000
Iron homeostasis					Creatine	-0.20	<0.0
	Iron <sup>a</sup>	-0.27	<0.0001	One carbon metabolism			
	Transferrin	-0.26	<0.0001		Dimethylamine	0.24	< 0.00
	saturation <sup>a</sup>				Trimethylamine	0.22	< 0.00
	Transferrin <sup>a</sup>	-0.10	ns		Glycine	-0.39	< 0.0000
Pulmonary function					Serine	-0.24	< 0.00
,	Dyspnea	-0.10	ns	TCA cycle			
	HF	-0.11	ns	•	Citric acid	-0.46	< 0.0000
	RR	-0.11	ns	AA and derivatives			
	O <sub>2</sub> saturation <sup>b</sup>	-0.03	ns		Aspartate	0.20	<0.0
Liver function	_				Threonine	-0.43	< 0.0000
	Urea <sup>c</sup>	0.12	ns		Alanine	-0.38	< 0.0000
	GGT <sup>a</sup>	0.06	ns		4-Hydroxyproline	-0.28	< 0.000
Kidney function					Glutamine	-0.22	< 0.00
,	Creatine <sup>a</sup>	0.06	ns	Urea cycle			
	GFR <sup>a</sup>	-0.11	ns	,	Allantoin	-0.28	<0.0
					Citrulline	-0.28	<0.000
Spearman's rank correlat					Arginine	-0.24	<0.00
deep red denotes +1, de	. •				Urea	-0.20	<0.0
correlation. BMI, body m	ass index: HOMA-IR.	homeostasis	s model	Other			0.0

assessment-insulin resistance; EASIX, endothelial activation and stress index; LDH, lactate dehydrogenase; INR, international normalised ratio; HF, heart frequency; RR, respiratory rate: GGT, gamma-glutamyl transferase; AST, aspartate aminotransferase; GFR, glomerular filtration rate. <sup>a</sup>Measured on the day of urine collection; <sup>b</sup>minimum value; <sup>c</sup>maximum value (peak).

accumulation of kynurenine metabolites could be a consequence of the virus-induced blockade of the downstream biochemical steps. In this view, the reduced urinary concentration of 1-methylnicotinamide and trigonelline could reflect an increased activation of the NAD+ salvage pathways, in an effort to improve NAD+ recycling. Therefore, a

Spearman's rank correlation; a color scale is used to illustrate r coefficients: deep red denotes +1, deep green denotes -1, white indicates no correlation. AA, amino acids; TCA, tricarboxylic acid.

0.27

-0.41

< 0.0001

< 0.0001

Pseudouridine

Erythritol

pilot study was performed to investigate whether the derangement in NAD+ biosynthesis could have influences on the activation of sirtuins, NAD+-consuming enzymes with potent immunomodulatory and antiviral properties.

We assessed SIRT1 expression in blood samples and found detectable concentrations of this enzyme only in 49

patients (presence of SIRT1), while 122 subjects showed no serum Sirt1 (absence of SIRT1). Next, we investigated the potential association between SIRT1 and the metabolic perturbations and clinical deterioration observed in COVID-19. Univariate analysis revealed that absence of SIRT1 was associated with significantly higher kynurenic acid, quinolinic acid, and neopterin levels in both serum and urine samples (Figure 6B). Moreover, patients with no SIRT1 expression had higher concentration of the inflammatory indexes ferritin, CRP, EASIX, and LDH compared with those patients showing detectable SIRT1 amounts in their blood (Figure 6C). Consistently, absence of SIRT1 was associated with increased serum concentration of the chemokines IL-8 and MCP-1 (Figure 6D).

#### Discussion

The present study confirms and expands the crucial role of urinary metabolic profiling as a diagnostic and prognostic tool in COVID-19. We show that changes in metabolite urinary concentration can stratify patients into classes of disease severity, with a discrimination ability comparable to that of clinical biomarkers. We likewise provide further evidence of the importance of the kynurenine pathway in SARS-CoV-2-induced phenoconversion, by documenting a marked accumulation of these metabolites in deteriorated patients as well as in higher-risk subjects. The analysis of urinary ddhNs indicates that these antiviral nucleosides not only describe active infection but are also associated with the main COVID-19-related perturbations, suggesting a potential role of such molecules as a molecular link between viral load, host immune response, and metabolic disturbances. Finally, an association between kynurenine dysregulations and NAD+/sirtuins has been established for the first time, offering a new pathogenic mechanism potentially responsible for a variety of COVID-19 pathological hallmarks.

By integrating <sup>1</sup>H NMR spectroscopy and LC-MS data, we provide a precise description of the changes in urine metabolite concentration associated with clinical deterioration and severe disease requiring patient hospitalization. More specifically, we identified 29 metabolites whose concentration significantly increases/decreases along with a worsening of clinical parameters routinely used to capture the main pathophysiological derangements of the disease [58, 59], including, CRP, SpO<sub>2</sub>, d-dimer, and lymphocyte count. In addition, in our cohort, metabolite urinary concentration showed a distinctive pattern in hospitalized and nonhospitalized individuals, with a diagnostic performance comparable to that of clinical variables. These observations further confirm that assessment of metabolite levels in urine

samples provides valuable diagnostic and prognostic information in COVID-19 [33,34,36,37] and could represent a potent mean for noninvasive screening in all the clinical conditions characterized by metabolic dysregulations. similarly to SARS-CoV-2 infection.

The greatest differences between higher-risk and lowerrisk patients were observed in the concentration of metabolites related to the tryptophan/kynurenine pathway and of the urinary ddhNs. SARS-CoV-2-induced dysregulation of the kynurenine pathway is widely described in both acute COVID-19 and PACS [17-24, 62]. The rise of kynurenines is positively associated with release of inflammatory mediators [18, 20, 23, 63] and disease severity [20, 23, 24]. Moreover, since high levels of kynurenic acid, 3-hydroxykynurenine, 3-hvdroxvanthranilic acid, and quinolinic acid exert deleterious effects on the brain and the gut [18, 39, 62], the accumulation of these molecules can directly contribute to exacerbating patient health status. Consistently, we found higher kynurenine urinary concentration in hospitalized patients compared with non-hospitalized, as well as in subjects showing poorer clinical picture. Moreover, increased tryptophan metabolites were detected in urine samples of higher-risk patients, including elderly and men. This finding offers a rationale for the poorer clinical outcome associated with these classes of patients [20, 23, 63].

Concerning ddhNs, our study provides additional information regarding their role in SARS-CoV-2 infection. In our previous work [32], we linked the excretion of these endogenous antiviral agents to the activity of the virus inhibitory protein, endoplasmic reticulum-associated, IFN inducible (Viperin) protein, an enzyme induced by interferons to inhibit viral replication [64]. A positive correlation between serum ddhNs and cytokine levels was also identified, together with higher ddhN urinary concentrations in hospitalized patients compared with nonhospitalized. Here, we confirm and expand these observations, by demonstrating that nucleoside concentration changes are associated with alterations in numerous clinical variables routinely used to assess patient health status in COVID-19, including biomarkers of inflammation, leukocyte count and molecules related to iron homeostasis. Moreover, the antiviral ddhNs showed a distinctive profile in hospitalized compared with nonhospitalized patients, with similar fold changes and statistical significance of CRP and ferritin. These findings clearly demonstrate that urinary ddhNs not only capture active viral infection but can also describe clinical deterioration, with a discrimination ability comparable with that of the markers currently used in clinical practice [58, 59]. With regard to associations with urinary metabolites, a strong positive correlation was found between ddhNs and neopterin, kynurenines, and taurine,

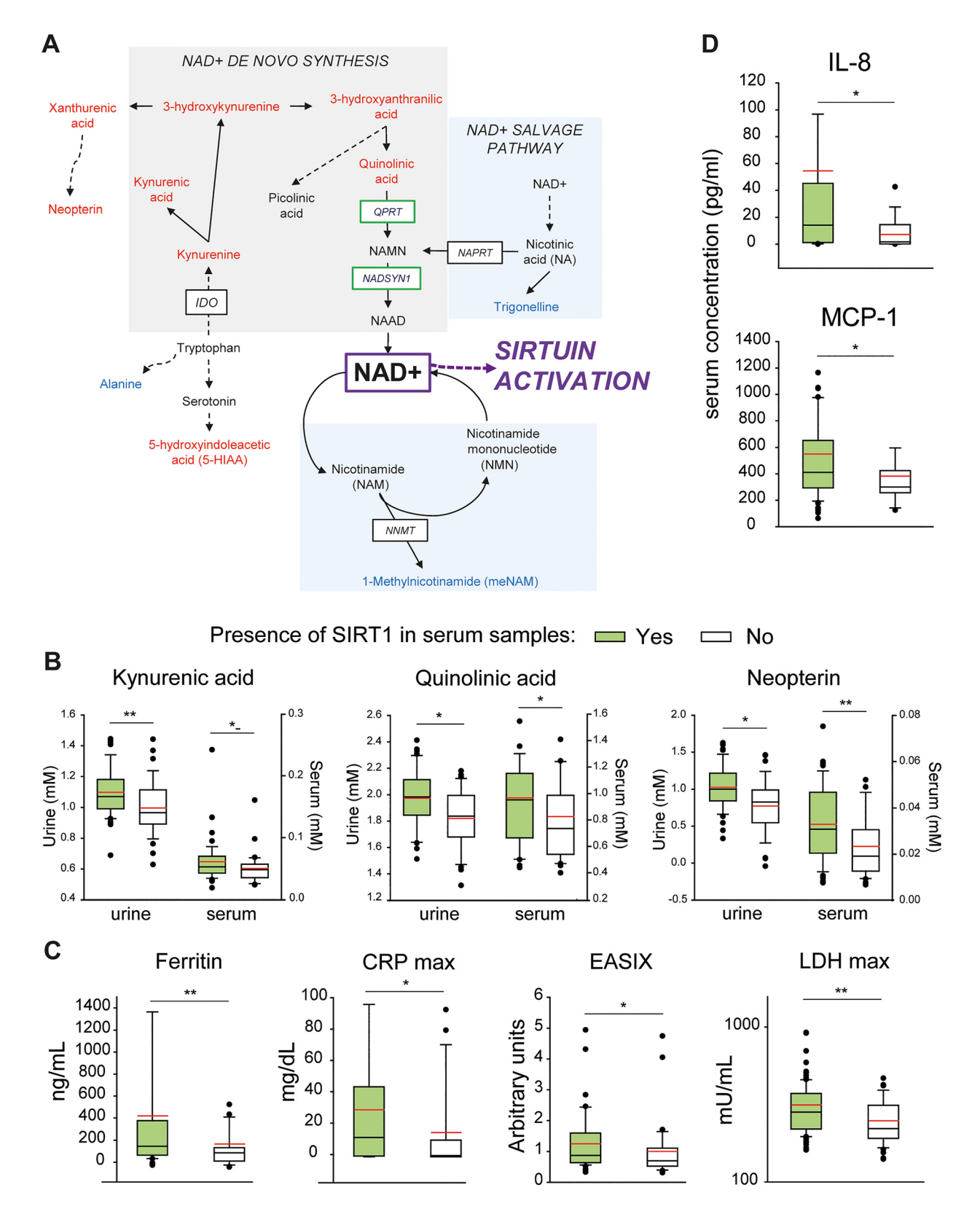


**Figure 6:** Association between kynurenine/trigonelline dysregulation, NAD<sup>+</sup> biosynthesis, and sirtuins. (A) Simplified diagram of the tryptophan pathway and its connection to NAD<sup>+</sup> biosynthesis, which, in turn, is crucial to activate sirtuins. Metabolites typed in red fonts have increased urinary concentrations in patients with worst clinical condition, in males, in elderly, and/or in subjects with higher ddhN urinary release, whereas metabolites typed in blue showed an opposite modulation pattern, with lower urinary concentrations in at least one of the patient classes mentioned above. Enzymes involved in

while different amino acids and molecules related to the urea cycle were inversely associated with the nucleosides. These results provide additional evidence supporting the connection between viral load, host antiviral response, and metabolic derangements in infectious diseases.

The comparison between AcuteCOV and controls, which relied exclusively on <sup>1</sup>H NMR data, further demonstrates that metabolic phenoconversion could have a causative role in the evolution of the main homeostatic perturbations observed in COVID-19 [18]. Increased succinate and fumarate, together with reduced citrate, denote an impairment in the TCA cycle, in line with previous studies [11, 33]. In particular, the rise of succinate suggests a dysfunctional mitochondrial complex II, namely succinate dehydrogenase, which plays a crucial role in the generation of oxygen reactive species [65-67]. Moreover, since succinate can act as a pro-inflammatory/ chemoattractant signaling molecule [26], its deregulation could represent one of the deleterious biological events leading to immunometabolic reprogramming, which was extensively documented in COVID-19 [5, 27]. Compared with noninfected individuals, the AcuteCOV group also showed reduced concentrations of dimethylamine, N,N-dimethylglycine, and glycine. In addition to being indicative of altered one-carbon metabolism, these findings could unveil a new-onset insulin resistance [68, 69]. The higher glucose excretion observed in SARS-CoV-2 patients further supports this concept [70, 71]. Consistent with previous papers [6, 18], we revealed a marked increase in urinary taurine. Accumulation of this metabolite could derive from deranged one-carbon/cysteine metabolism or might reflect the activation of adaptive mechanisms to cope with oxidative stress. Of note, taurine appears to be particularly relevant for PACS development, as perturbations in its concentration were reported to be persistently sustained over months after the original SARS-CoV-2 infection [6, 72].

The last section of our research sought to expand knowledge about SARS-CoV-2-induced changes in tryptophan metabolites and their involvement in the pathogenesis of COVID-19. From a mechanistic point of view, the kynurenine pathway leads to the production of quinolinic acid which, in turn, serves as a precursor in NAD+ de novo biosynthesis [38, 39, 73]. Besides being a key coenzyme in many redox reactions, NAD+ has emerged as a master regulator of inflammation, leukocyte functions, and host

antiviral responses [73–76]. In fact, NAD<sup>+</sup> availability is essential to activate the NAD<sup>+</sup>-dependent enzymes sirtuins, CD38, and poly-ADP-ribose polymerases (PARPs), which exert broad immunomodulatory and defense effects [40–44]. Increasing evidence demonstrates that many viruses, including SARS-CoV-2, can deplete NAD<sup>+</sup> concentrations [5, 77, 78]. This phenomenon could be part of the miscellaneous viral strategies to evade the host immune system [73, 79, 80]. Recently, Heer and colleagues showed that SARS-CoV-2 infection is associated with down-regulation of genes involved in NAD+ synthesis from tryptophan or nicotinic acid, namely QPRT and NADSYN [61]. Based on these findings, we hypothesized that the kynurenine accumulation detected in our cohort and in other AcuteCOV populations reflects a virus-induced blockade of the downstream biochemical steps required to generate NAD<sup>+</sup>. Furthermore, the reduced excretion of the niacin metabolite trigonelline could be a consequence of enhanced NAD<sup>+</sup> recycling in the salvage pathways. Since NAD+ depletion leads to decreased sirtuin activity [43], we tested the idea that such SARS-CoV-2-induced metabolic perturbations could be associated with SIRT1 deregulation.

Our pilot study discloses, for the first time, a potential association between kynurenines/trigonelline and SIRT1 in COVID-19. In fact, higher kynurenine concentrations in both serum and urine samples were associated with lower SIRT1 blood levels. After stratifying our cohort according to SIRT1 levels, we found that patients with impaired SIRT1 showed higher serum concentration of biomarkers of systemic inflammation and epithelial dysfunction, as well as an enhanced release of inflammatory mediators. Given the multiple detrimental consequences of SIRT1 deregulation on host homeostasis [41, 42, 81], our preliminary results not only provide a potential mechanistic explanation underlying the SARS-CoV-2-induced superactivation of the kynurenine pathway, but they also offer a new pathogenic mechanism potentially responsible for a variety of clinical manifestations in COVID-19, including excessive systemic cytokine release, metabolism alterations, and insulin resistance.

Some limitations of the study should be discussed. First, this is a single-center analysis which mainly involved patients suffering from mild disease, while a very small proportion of severe cases was included [46]. Therefore, the results of the present research could not be generalized to

the biochemical reactions presented here are typed in capital letters; the expression of enzymes framed in green is modulated by SARS-CoV-2 [61]. Differences in the concentration of (B) selected metabolites, (C) clinical variables, and (D) serum inflammatory mediators between patient groups derived based on absence (n=122, white box) or presence (n=49, green box) of SIRT1 in serum samples. Box plots illustrate median [25–75], red lines denote the mean of each study group. Wilcoxon-Mann-Whitney test; p-values: \*p<0.05; \*\*p<0.01; \*\*\*p<0.001. CRP, C-reactive protein; EASIX, endothelial activation and stress index; LDH, lactate dehydrogenase; IDO, 2,3-dioxygenase and indole 2,3-dioxygenase; NADSYN1, NAD synthetase 1; NAPRT, nicotinic acid phosphoribosyltransferase; NNMT, nicotinamide N-methyltransferase; QPRT, quinolate phosphoribosyltransferase; SIRT1, sirtuin 1.

the wide-spectrum of COVID-19 severity classes. On the other hand, our data specifically describe the metabolic perturbations underlying asymptomatic and mild diseases, which, due to the successful introduction of vaccination, represent the most common clinical manifestations of SARS-CoV-2 infection. Second, we exclusively analyzed spontaneous urine that could be less informative than 24 h-urine in describing a person's metabolic state as it is affected by external factors such as diet, hydration, and circadian rhythms. Nevertheless, compared to 24-h urine, spontaneous urine samples offer clear clinical advantages in terms of ease of collection and practicality. Hence, they were considered the optimal choice for analyzing a large number of patients in our real-world cohort. Still on sample collection, since the "Coronataxi" study did not involve scheduled regimen for collecting biological specimens, we cannot exclude the possibility of influences on the urinary metabolite profile due to variations in fasting condition among patients. Lastly, we acknowledge that evaluating SIRT1 concentration by ELISA may not represent the ideal method to investigate Sirtuin activation. Despite this, we were able to provide preliminary evidence suggesting a potential link between the kynurenine pathway and NAD+/sirtuins in SARS-CoV-2. Therefore, our results represent a useful starting point for further researches on the topic.

In conclusion, we demonstrated that urinary metabolomics assumes similar diagnostic/prognostic power to clinical pathology in COVID-19 as it can fully capture patient clinical deterioration and aberrant immune activation. Therefore, the description of metabolite changes in urine samples appears extremely useful not only to optimize patient stratification, but also to assess the effectiveness of novel treatments in preventing severe COVID-19 or PACS development. In this regard, the urinary ddhNs emerge as promising biomarkers of SARS-CoV-2 and possibly other viral infections. In fact, unlike the nonspecific markers currently used in the clinical practice, ddhNs concentration is not influenced by pre-existing comorbidities. To facilitate the clinical usability of our results, Table 5 provides a list of the most discriminant metabolites for each of our study aims, along with their absolute concentrations. The combined use of serum and urine metabolomics can further improve diagnostic accuracy, fostering the application of precision medicine in the context of infectious diseases [82], as well as in other clinical conditions marked by deranged metabolism.

A substantial novelty of the present research resides in the recognition of a potential association between kynurenine pathway superactivation and impaired NAD<sup>+</sup> biosynthesis, which could lead to inefficient sirtuin response. Our

Table 5: Most discriminant metabolites.

Metabolite	Normalized concentration, mM								
	Aim 1		Aim 2 – hospitalization		Aim 3 – Total ddhNs		Aim 4 – Serum SIRT1		
	AcuteCOV	CTR	Yes	No	High	Low	Presence	Absence	
3-Hydroxykynurenine	NA	NA	31.82 ± 7.53	7.90 ± 3.42	11.19 ± 13.94	3.91 ± 16.7	$0.08 \pm 0.13^{a}$	$0.10 \pm 0.00^{a}$	
Acetone	$0.05 \pm 0.09$	$0.03 \pm 0.00$							
Alanine	NA	NA			266.6 ± 105.3	383.2 ± 116.7	356.2 ± 165.0	296.3 ± 135.9	
Citric acid	$2.96 \pm 2.39$	4.57 ± 1.23	2.73 ± 1.13	$4.79 \pm 2.17$	1.29 ± 1.01	$2.88 \pm 1.43$			
Creatine	$0.52 \pm 2.25$	$1.38 \pm 0.01$							
DdhC	NA	NA	$3,457 \pm 948$	$2052 \pm 956$	NA	NA			
Glucose	$0.78 \pm 1.42$	$0.28 \pm 0.03$			1.07 ± 1.15	$0.45 \pm 0.24$			
Glycine	$1.34 \pm 1.02$	$1.72 \pm 0.34$	1751 ± 643	$2602 \pm 1,694$	$924 \pm 401$	$1473 \pm 835$	1494 ± 1,065	$1085 \pm 811$	
Hippuric acid	1.72 ± 2.21	$3.37 \pm 0.75$							
Kynurenine	NA	NA	26.56 ± 11.36	$8.59 \pm 2.33$	$16.78 \pm 14.72$	$3.41 \pm 4.45$	$1.65 \pm 0.75^{a}$	$2.01 \pm 0.34^{a}$	
Neopterin	NA	NA	24.87 ± 15.55	19.01 ± 15.37	17.25 ± 11.12	$3.66 \pm 2.83$	$9.05 \pm 6.72$	$12.49 \pm 8.82$	
Picolinic acid	NA	NA					$1.67 \pm 0.94$	$1.31 \pm 0.73$	
Quinolinic acid	NA	NA			123.23 ± 59.53	$48.53 \pm 24.25$	$63.62 \pm 24.44$	$95.52 \pm 50.6$	
Succinic acid	$0.12 \pm 0.07$	$0.08\pm0.00$					$0.11 \pm 0.10$	$0.08 \pm 0.03$	
Taurine	1.66 ± 1.16	$0.98 \pm 0.02$	$3484 \pm 2023$	2664 ± 1721	$1952 \pm 806$	999 ± 421			
Trigonelline	$0.31 \pm 0.34$	$0.46\pm0.20$	$0.32 \pm 0.2$	$0.57 \pm 0.20$	$0.11 \pm 0.11$	$0.32 \pm 0.27$			

Summary Table reporting the average normalized concentration of the metabolites showing the highest fold change/statistical significance in one of the following comparison: (1) Aim 1, AcuteCOV vs. CTR; (2) Aim 2, hospitalized patients vs. nonhospitalized patients; (3) Aim 3, high "Total ddhNs" vs. low "Total ddhNs"; (4) Aim 4, presence of SIRT1 in serum samples vs. absence of SIRT1 in serum samples. Normalized concentrations were obtained by applying the probabilistic quotient normalization (PQN); data are presented as mean ± SD NA, not applicable. aSerum metabolite.

observations could be of paramount clinical relevancefor the development of innovative therapeutic strategies aimed at restoring the physiological NAD+ turnover in COVID-19 patients [75, 83, 84].

Acknowledgments: The authors acknowledge the Werner Siemens Foundation for supporting this project. Caterina Lonati wishes to express her gratitude to Dr. Stefano Gatti for his valuable guidance and support. She also thanks Fondazione IRCCS Ca' Granda Ospedale Maggiore Policlinico for the financial support (Ricerca Corrente 2021, grant number 060/15). Research ethics: SARS-CoV-2 positive individuals were recruited from 7th September 2020 to 21st March 2021 within a prospective non-interventional study conducted by Heidelberg University Hospital (Lim et al. 2022). According to the World Health Organization (WHO) guidance, laboratory confirmation for SARS-CoV-2 was defined as a positive result of quantitative real-time reverse transcriptase-polymerase chain reaction (gRT-PCR) assay of nasal and pharyngeal swabs. Only subjects who were over 18 years of age and showing completed questionnaires were included. The local Ethics committee had approved biosample and data collection and analysis (reference number: S-324/2020).

**Informed consent:** All participants provided written informed consent according to the Declaration of Helsinki. Author contributions: Conceptualization: CL, CT, JW, JN; Methodology: NG, NL, SL; Software: GB, NG, RM, SL, JW; Formal Analysis: CL, SS, PN, NL, NG, RM, SL, JW, GB; Investigation: AK, SS, PN, NG, NL, GB; Data Curation: CL, AK, SL, RM, GB; Visualization: CL; Writing - Original Draft: CL; Writing, Review and Editing: SS, RM, SL, AK, GB, YS, LZ, CT; Supervision: JW, JN, CT; Funding Acquisition: [W, JN, CT. All authors discussed the results and revised the final version of the manuscript.

**Competing interests:** CT and GB report a research grant from Bruker BioSpin GmbH. CH and HH are employed at Bruker BioSpin GmbH. Their role is consisted in providing access to IVDr SOPs and spectral analysis tool without having any influence on the study design or results of this study. All other authors declare no competing interests.

Research funding: Werner Siemens Foundation: Werner Siemens Imaging Center.

Data availability: Mean metabolite concentrations with standard deviations as well as raw spectral data will be made available upon request.

#### References

- 1. World Health Organization. WHO coronavirus (COVID-19) dashboard. [Internet]. Available from: https://covid19.who.int.
- 2. Phillips N. The coronavirus will become endemic. Nature 2021;590:382-4.

- 3. Nalbandian A, Sehgal K, Gupta A, Madhavan MV, McGroder C, Stevens JS, et al. Post-acute COVID-19 syndrome. Nat Med [Internet] 2021;27:601-15.
- 4. Lonati C, Gatti S, Catania A. Activation of melanocortin receptors as a potential strategy to reduce local and systemic reactions induced by respiratory viruses. Front Endocrinol 2020;11:569241.
- 5. Xiao N, Nie M, Pang H, Wang B, Hu J, Meng X, et al. Integrated cytokine and metabolite analysis reveals immunometabolic reprogramming in COVID-19 patients with therapeutic implications. Nat Commun 2021;12: 1-13.
- 6. Holmes E, Wist J, Masuda R, Lodge S, Nitschke P, Kimhofer T, et al. Incomplete systemic recovery and metabolic phenoreversion in postacute-phase nonhospitalized COVID-19 patients: implications for assessment of post-acute COVID-19 syndrome; | Proteome Res 2021;20:
- 7. Fung S-Y, Yuen K-S, Ye Z-W, Chan C-P, Jin D-Y. A tug-of-war between severe acute respiratory syndrome coronavirus 2 and host antiviral defence: lessons from other pathogenic viruses. Emerg Microb Infect 2020;9:558-70.
- 8. Bellocchio F, Carioni P, Lonati C, Garbelli M, Martínez-Martínez F, Stuard S, et al. Enhanced sentinel surveillance system for covid-19 outbreak prediction in a large european dialysis clinics network. Int J Environ Res Publ Health 2021;18:9739.
- Sindelar M, Stancliffe E, Schwaiger-Haber M, Anbukumar DS, Adkins-Travis K, Goss CW, et al. Longitudinal metabolomics of human plasma reveals prognostic markers of COVID-19 disease severity. Cell Reports Med 2021;2:100369.
- 10. Pang Z, Zhou G, Chong J, Xia J. Comprehensive meta-analysis of covid-19 global metabolomics datasets. Metabolites 2021;11:1-14.
- 11. Rössler T, Berezhnoy G, Singh Y, Cannet C, Reinsperger T, Schäfer H, et al. Quantitative serum NMR spectroscopy stratifies COVID-19 patients and sheds light on interfaces of host metabolism and the immune response with cytokines and clinical parameters. Metabolites 2022;12:1277.
- 12. Bruzzone C, Conde R, Embade N, Mato JM, Millet O. Metabolomics as a powerful tool for diagnostic, pronostic and drug intervention analysis in COVID-19. Front Mol Biosci 2023:10:1-11.
- 13. Mussap M, Fanos V. Could metabolomics drive the fate of COVID-19 pandemic? A narrative review on lights and shadows. Clin Chem Lab Med 2021;59:1891-905.
- 14. Su Y, Chen D, Yuan D, Lausted C, Choi J, Dai CL, et al. Multi-Omics resolves a sharp disease-state shift between mild and moderate COVID-19. Cell 2020;183:1479-95.e20.
- 15. Bruzzone C, Bizkarguenaga M, Gil-Redondo R, Diercks T, Arana E, García de Vicuña A, et al. SARS-CoV-2 infection dysregulates the metabolomic and lipidomic profiles of serum. iScience 2020;23:101645.
- 16. Lodge S, Nitschke P, Kimhofer T, Coudert JD, Begum S, Bong SH, et al. NMR spectroscopic windows on the systemic effects of SARS-CoV-2 infection on plasma lipoproteins and metabolites in relation to circulating cytokines. J Proteome Res. 2021;20:1382-96.
- 17. Danlos FX, Grajeda-Iglesias C, Durand S, Sauvat A, Roumier M, Cantin D, et al. Metabolomic analyses of COVID-19 patients unravel stagedependent and prognostic biomarkers. Cell Death Dis [Internet] 2021; 12:258. https://doi.org/10.1038/s41419-021-03540-y.
- 18. Lawler NG, Gray N, Kimhofer T, Boughton B, Gay M, Yang R, et al. Systemic perturbations in amine and kynurenine metabolism associated with acute SARS-CoV - 2 infection and inflammatory cytokine responses. J Proteome Res 2021;20:2796-811.
- 19. Dewulf JP, Martin M, Marie S, Oguz F, Belkhir L, De Greef J, et al. Urine metabolomics links dysregulation of the tryptophan-kynurenine pathway to inflammation and severity of COVID-19. Sci Rep 2022;12:1-8.

- 20. Cai Y, Kim DJ, Takahashi T, Broadhurst DI, Yan H, Ma S, et al. Kynurenic acid may underlie sex-specific immune responses to COVID-19. Sci Signal 2021;14:1-12.
- 21. Bizjak DA, Stangl M, Börner N, Bösch F, Durner J, Drunin G, et al. Kynurenine serves as useful biomarker in acute, Long- and Post-COVID-19 diagnostics. Front Immunol 2022;13:1-11.
- 22. Shen B, Yi X, Sun Y, Bi X, Du J, Zhang C, et al. Proteomic and metabolomic characterization of COVID-19 patient sera. Cell 2020;182:
- 23. Thomas T, Stefanoni D, Reisz JA, Nemkov T, Bertolone L, Francis RO, et al. COVID-19 infection alters kynurenine and fatty acid metabolism, correlating with IL-6 levels and renal status. JCI Insight 2020;5:e140327.
- 24. Roberts I, Wright Muelas M, Taylor JM, Davison AS, Xu Y, Grixti JM, et al. Untargeted metabolomics of COVID-19 patient serum reveals potential prognostic markers of both severity and outcome. Metabolomics [Internet] 2022;18:1-19.
- 25. Caterino M, Costanzo M, Fedele R, Cevenini A, Gelzo M, Di Minno A, et al. The serum metabolome of moderate and severe covid-19 patients reflects possible liver alterations involving carbon and nitrogen metabolism. Int J Mol Sci 2021;22:1-18.
- 26. Ryan DG, Murphy MP, Frezza C, Prag HA, Chouchani ET, O'Neill LA, et al. Coupling Krebs cycle metabolites to signalling in immunity and cancer. Nat Metab2019;1:16-33.
- 27. Batabyal R, Freishtat N, Hill E, Rehman M, Freishtat R, Koutroulis I. Metabolic dysfunction and immunometabolism in COVID-19 pathophysiology and therapeutics. Int J Obes. 2021;45:1163-9.
- 28. Otvos JD, Shalaurova I, Wolak-Dinsmore J, Connelly MA, Mackey RH, Stein JH, et al. GlycA: a composite nuclear magnetic resonance biomarker of systemic inflammation. Clin Chem 2015;61:714-23.
- 29. Masuda R, Lodge S, Whiley L, Gray N, Lawler N, Nitschke P, et al. Exploration of human serum lipoprotein supramolecular phospholipids using statistical heterospectroscopy in n – dimensions (SHY-n): identi fi cation of potential cardiovascular risk biomarkers related to SARS-CoV-2 infection. Anal Chem 2022;94:4426-36.
- 30. Nicholson JK. Molecular phenomic approaches to deconvolving the systemic effects of SARS-CoV-2 infection and post-acute COVID-19 syndrome. Phenomics. 2021;1:143-50.
- 31. Holmes E, Nicholson JK, Lodge S, Nitschke P, Kimhofer T, Wist J, et al. Diffusion and relaxation edited proton NMR spectroscopy of plasma reveals a high-fidelity supramolecular biomarker signature of SARS-CoV-2 infection. Anal Chem 2021;93:3976-86.
- 32. Sala S, Nitschke P, Masuda R, Gray N, Lawler N, Wood JM, et al. SARS-CoV-2 infection biomarkers reveal an extended RSAD2 dependant metabolic pathway. medRxiv 2023. https://doi.org/10.1101/2023.05.08. 23289637.
- 33. Baiges-Gaya G, Iftimie S, Castañé H, Rodríguez-Tomàs E, Jiménez-Franco A, López-Azcona AF, et al. Combining semi-targeted metabolomics and machine learning to identify metabolic alterations in the serum and urine of hospitalized patients with COVID-19. Biomolecules 2023;13:163.
- 34. Marhuenda-Egea FC, Narro-Serrano J, Shalabi-Benavent MJ, Álamo-Marzo JM, Amador-Prous C, Algado-Rabasa JT, et al. A metabolic readout of the urine metabolome of COVID-19 patients. Metabolomics [Internet] 2023;19:7.
- 35. Morell-Garcia D, Ramos-Chavarino D, Bauça JM, Argente del Castillo P, Ballesteros-Vizoso MA, García de Guadiana-Romualdo L, et al. Urine biomarkers for the prediction of mortality in COVID-19 hospitalized patients. Sci Rep [Internet] 2021;11:1-13.

- 36. Bi X, Liu W, Ding X, Liang S, Zheng Y, Zhu X, et al. Proteomic and metabolomic profiling of urine uncovers immune responses in patients with COVID-19. Cell Rep [Internet]. 2022;38:110271.
- 37. Rosolanka R, Liptak P, Baranovicova E, Bobcakova A, Vysehradsky R, Duricek M, et al. Changes in the urine metabolomic profile in patients recovering from severe COVID-19. Metabolites 2023;13:364.
- 38. Fletcher RS, Lavery GG. The emergence of the nicotinamide riboside kinases in the regulation of NAD+ metabolism. J Mol Endocrinol 2018;
- 39. Moffett JR, Arun P, Puthillathu N, Vengilote R, Ives JA, Badawy AAB, et al. Quinolinate as a marker for kynurenine metabolite formation and the unresolved question of NAD+ synthesis during inflammation and infection. Front Immunol 2020;11:1-27.
- 40. Koyuncu E, Budayeva HG, Miteva YV, Ricci DP, Silhavy TJ, Shenk T, et al. Sirtuins are evolutionarily conserved viral restriction factors. mBio 2014:5:1-10.
- 41. Preyat N, Leo O. Sirtuin deacylases: a molecular link between metabolism and immunity. J Leukoc Biol 2013;93:669-80.
- 42. Wu QJ, Zhang TN, Chen HH, Yu XF, Lv JL, Liu YY, et al. The sirtuin family in health and disease. Signal Transduct Targeted Ther 2022;7:402.
- 43. Yang Y, Liu Y, Wang Y, Chao Y, Zhang J, Jia Y, et al. Regulation of SIRT1 and its roles in inflammation. Front Immunol 2022;13:1-16.
- 44. Poulose N, Raju R. Sirtuin regulation in aging and injury. Biochim Biophys Acta - Mol Basis Dis [Internet] 2015;1852:2442-55.
- 45. Algarni MH, Foudah AI, Muharram MM, Labrou NE. The pleiotropic function of human sirtuins as modulators of metabolic pathways and viral infections. Cells 2021;10:1-20.
- 46. Lim A, Hippchen T, Unger I, Heinze O, Welker A, Kräusslich HG, et al. An outpatient management strategy using a Coronataxi digital early warning system reduces coronavirus disease 2019 mortality. Open Forum Infect Dis 2022;9:ofac063.
- 47. Embade N, Cannet C, Diercks T, Gil-Redondo R, Bruzzone C, Ansó S, et al. NMR-based newborn urine screening for optimized detection of inherited errors of metabolism. Sci Rep 2019;9:1-9.
- 48. Bae G, Berezhnoy G, Koch A, Cannet C, Schäfer H, Kommoss S, et al. Stratification of ovarian cancer borderline from high-grade serous carcinoma patients by quantitative serum NMR spectroscopy of metabolites, lipoproteins, and inflammatory markers. Front Mol Biosci 2023;10:1-18.
- 49. Dona AC, Jiménez B, Schafer H, Humpfer E, Spraul M, Lewis MR, et al. Precision high-throughput proton NMR spectroscopy of human urine, serum, and plasma for large-scale metabolic phenotyping. Anal Chem 2014;86:9887-94.
- 50. Cloarec O, Dumas ME, Craig A, Barton RH, Trygg J, Hudson J, et al. Statistical total correlation spectroscopy: an exploratory approach for latent biomarker identification from metabolic 1H NMR data sets. Anal Chem 2005;77:1282-9.
- 51. Akoka S, Barantin L, Trierweiler M. Concentration measurement by proton NMR using the ERETIC method. Anal Chem 1999;71:2554-7.
- 52. Wider G, Dreier L. Measuring protein concentrations by NMR spectroscopy. J Am Chem Soc 2006;128:2571-6.
- 53. Gray N, Lawler NG, Yang R, Morillon AC, Gay MCL, Bong SH, et al. A simultaneous exploratory and quantitative amino acid and biogenic amine metabolic profiling platform for rapid disease phenotyping via UPLC-QToF-MS. Talanta 2021;223:121872.
- 54. Vollmar AKR, Rattray NJW, Cai Y, Santos-Neto ÁJ, Deziel NC, Jukic AMZ, et al. Normalizing untargeted periconceptional urinary metabolomics data: a comparison of approaches. Metabolites 2019;9:198.

- 55. Benjamini Y, Hochberg Y. Controlling the false discovery rate: a practical and powerful approach to multiple testing author (s): Yoav Benjamini and Yosef Hochberg source: Journal of the royal statistical society. Series B (methodological), Vol. 57, No. 1 (1995), Publi. J R Stat Soc 1995;57:289-300.
- 56. Geifman N, Cohen R, Rubin E. Redefining meaningful age groups in the context of disease. Age (Omaha). 2013;35:2357-66.
- 57. Weir CB, Ian A, BMI classification percentile and cut off points [Internet]. Treasure island (FL): StatPearls Publishing; 2022. Available from: https://www.ncbi.nlm.nih.gov/books/ NBK541070/.
- 58. Miller JL, Tada M, Goto M, Chen H, Dang E, Mohr NM, et al. Prediction models for severe manifestations and mortality due to COVID-19: a systematic review. Acad Emerg Med 2022;29:206-16.
- 59. Cavallazzi R, Bradley J, Chandler T, Furmanek S, Ramirez JA. Severity of illness scores and biomarkers for Prognosis of patients with coronavirus disease 2019. Semin Respir Crit Care Med 2023;44:75-90.
- 60. Luft T, Wendtner CM, Kosely F, Radujkovic A, Benner A, Korell F, et al. EASIX for prediction of outcome in hospitalized SARS-CoV-2 infected patients. Front Immunol 2021;12:1-9.
- 61. Heer CD, Sanderson DJ, Voth LS, Alhammad YMO, Schmidt MS, Trammell SAI, et al. Coronavirus infection and PARP expression dysregulate the NAD metabolome: an actionable component of innate immunity. J Biol Chem [Internet] 2020;295:17986-96.
- 62. Blackett JW, Sun Y, Purpura L, Margolis KG, Elkind MSV, O'Byrne S, et al. Decreased gut microbiome tryptophan metabolism and serotonergic signaling in patients with persistent mental health and gastrointestinal symptoms after COVID-19. Clin Transl Gastroenterol 2022:13:e00524.
- 63. Escarcega RD, Honarpisheh P, Colpo GD, Ahnstedt HW, Couture L, Juneja S, et al. Sex differences in global metabolomic profiles of COVID-19 patients. Cell Death Dis 2022;13:461.
- 64. Seo JY, Yaneva R, Hinson ER, Cresswell P. Human cytomegalovirus directly induces the antiviral protein viperin to enhance infectivity. Science 2011;332:1093-7.
- 65. Chouchani ET, Pell VR, James AM, Work LM, Saeb-Parsy K, Frezza C, et al. A unifying mechanism for mitochondrial superoxide production during ischemia-reperfusion injury. Cell Metabol 2016;23:254-63.
- 66. Lonati C, Dondossola D, Zizmare L, Battistin M, Wüst L, Vivona L, et al. Quantitative metabolomics of tissue, Perfusate, and bile from rat livers subjected to Normothermic machine Perfusion. Biomedicines 2022;10:
- 67. Tretter L, Patocs A, Chinopoulos C. Succinate, an intermediate in metabolism, signal transduction, ROS, hypoxia, and tumorigenesis. Biochim Biophys Acta Bioenerg 2016;1857:1086–101.
- 68. Palau-Rodriguez M, Tulipani S, Queipo-Ortuño MI, Urpi-Sarda M, Tinahones FJ, Andres-Lacueva C. Metabolomic insights into the intricate gut microbial-host interaction in the development of obesity and type 2 diabetes. Front Microbiol 2015;6:1-12.

- 69. Guan M, Xie L, Diao C, Wang N, Hu W, Zheng Y, et al. Systemic perturbations of key metabolites in diabetic rats during the evolution of diabetes studied by urine metabonomics. PLoS One 2013;8:1-10.
- 70. He X, Liu C, Peng J, Li Z, Li F, Wang J, et al. COVID-19 induces new-onset insulin resistance and lipid metabolic dysregulation via regulation of secreted metabolic factors. Signal Transduct Targeted Ther 2021;6:427. https://doi.org/10.1038/s41392-021-00822-x.
- 71. Govender N. Khalig OP, Moodley I, Naicker T, Insulin resistance in COVID-19 and diabetes. Prim Care Diabetes 2021;15:629-34.
- 72. Zhang S, Luo P, Xu J, Yang L, Ma P, Tan X, et al. Plasma metabolomic profiles in recovered covid-19 patients without previous underlying diseases 3 months after discharge. J Inflamm Res 2021;14:
- 73. Mesquita I, Varela P, Belinha A, Gaifem J, Laforge M, Vergnes B, et al. Exploring NAD+ metabolism in host-pathogen interactions. Cell Mol Life Sci 2016;73:1225-36.
- 74. Billingham LK, Chandel NS. NAD-biosynthetic pathways regulate innate immunity. Nat Immunol 2019;20:380-2.
- 75. Zheng M, Schultz MB, Sinclair DA. NAD+ in COVID-19 and viral infections. Trends Immunol 2022;43:283-95.
- 76. Minhas PS, Liu L, Moon PK, Joshi AU, Dove C, Mhatre S, et al. Macrophage de novo NAD+ synthesis specifies immune function in aging and inflammation. Nat Immunol 2019;20:50-63.
- 77. Blasco H, Bessy C, Plantier L, Lefevre A, Piver E, Bernard L, et al. The specific metabolome profiling of patients infected by SARS-COV-2 supports the key role of tryptophan-nicotinamide pathway and cytosine metabolism. Sci Rep 2020;10:1-12.
- 78. Rahimmanesh I, Kouhpayeh S, Azizi Y, Khanahmad H. Conceptual framework for SARS-CoV-2 - related lymphopenia. Adv Biomed Res 2022:11:16
- 79. Grunewald ME, Chen Y, Kuny C, Maejima T, Lease R, Ferraris D, et al. The coronavirus macrodomain is required to prevent PARP-mediated inhibition of virus replication and enhancement of IFN expression. PLoS Pathog [Internet] 2019;15:1-24.
- 80. Kikkert M. Innate immune evasion by human respiratory RNA viruses. I Innate Immun 2020:12:4-20.
- 81. Elibol B, Kilic U. High levels of SIRT1 expression as a protective mechanism against disease-related conditions. Front Endocrinol 2018;9:1-7.
- 82. Ward RA, Aghaeepour N, Bhattacharyya RP, Clish CB, Gaudillière B, Hacohen N, et al. Harnessing the potential of multiomics studies for precision medicine in infectious disease. Open Forum Infect Dis 2021;8:1-12.
- 83. Rajman L, Chwalek K, Sinclair DA. Therapeutic potential of NADboosting molecules: the In Vivo evidence. Cell Metab 2018;27:529-47.
- 84. Mueller AL, Mcnamara MS, Sinclair DA. Why does COVID-19 disproportionately affect older people? Aging 2020;12:9959-81.

Supplementary Material: This article contains supplementary material (https://doi.org/10.1515/cclm-2023-1017).